Chapter 10
Planetary Entry

10.1 Introduction

After a spaceflight, the planetary entry (a.k.a. reentry for entry into Earth's atmosphere) of a spacecraft is subject to the same aerodynamic and physical laws and equations (see Eqs. (6.3.6) and (6.3.7)) as ascent. One might therefore infer that the circumstances of both situations are the same. But they actually differ vastly due to the initial and boundary conditions: At launch we have $h = 0, v = 0$ at flight path angle $\gamma = 90°$ and full thrust during ascent, while at reentry it is exactly the other way round, $h \approx 350$ km, $v \approx 7.9$ km/s, $\gamma \approx 0°$, and no thrust. Owing to these converse initial conditions the S/C in LEO prior to reentry possesses a high amount of potential and kinetic energy of approximately 33 MJ kg^{-1}. This energy has to be annihilated during reentry in a controlled way and in a relatively short period of time, while the structural load on the vehicle needs to be kept within limits. In face of this problem there are four critical parameters to be considered when designing a vehicle for atmospheric reentry to avoid damage to the S/C and the crew:

- Peak heat flux
- Heat load
- Peak deceleration
- Peak dynamic pressure

Peak heat flux (heat per unit area and unit time = heat flow density) selects the thermal protection material, while heat load selects the thickness of the protection material stack. Peak deceleration is of major importance for the crew and should not exceed 8 g. Dynamic pressure causes aerodynamic stress load to the vehicle and is significant in particular for winged bodies: The Shuttle was designed for 2.5 g load while Apollo for a 12 g load. In total, these constraints impose boundaries on the reentry trajectory, which are depictured for a Shuttle reentry in Fig. 10.1.

U. Walter, *Astronautics*, https://doi.org/10.1007/978-3-319-74373-8_10

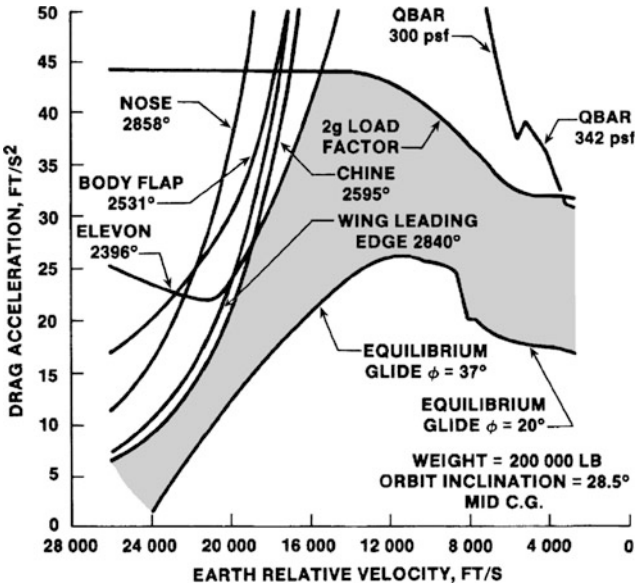

Fig. 10.1 Representative constraint boundaries (English units, temperature in Fahrenheit) for a Space Shuttle reentry shaping a reentry corridor (gray). *Credit* N. Chaffee, NASA/JSC

In summary, the deceleration force causing stress load to the vehicle structure and crew plus the heat load to the thermal protection system are the essential physical quantities, which need to be examined for a reentry as done in this chapter.

10.1.1 Aerothermodynamical Challenges

Aerothermodynamics investigates the heat flux onto the vehicle and the subsequent heating of the spacecraft's surface. During reentry this is caused by the annihilation of the low Earth orbital energy, which essentially is the kinetic energy $E_{tot} \approx \frac{1}{2}mv^2 = \frac{1}{2}mg_0\, R_\oplus \approx 33$ MJ kg^{-1}. The following rough estimate shows that this heat flux and surface heating is tremendous, and keeping the heat in given limits is not easy to accomplish.

A capsule in the so-called ballistic reentry (see Sect. 10.3.2) for aerobraking converts its orbital energy into frictional heat, which is released as a heat flow rate $\dot{Q} = E_{tot}/\tau$ within typically $\tau \approx 0.5$ min. Usually 99.9% of that is released via heat convection to the air flow. The rest, sometimes called convective heat flux, which is quantified by the so-called Stanton number St and having roughly the universal value of $St \approx 0.1\%$, is taken up by the surface of the S/C. The thermal shield of the S/C with an area of A and with emissivity of typically $\varepsilon \approx 0.85$ then radiates away

the absorbed heat with a heat flux $\dot{q}_{S/C}$, which according to the Stefan-Boltzmann law is related to the shield temperature T

$$T^4 = \frac{\dot{Q}}{\varepsilon\sigma A} = \frac{\dot{q}_{S/C}}{\varepsilon\sigma} \tag{10.1.1}$$

with the Stefan–Boltzmann constant $\sigma = 5.6705 \times 10^{-8}$ W m^{-2} K^{-4}. When the thermal shield is in thermal balance, we get the following from the above considerations:

$$St\frac{E_{tot}}{\tau} = St\frac{mg_0R_\oplus}{2\tau} = A\varepsilon\sigma T^4 \tag{10.1.2}$$

Example 1

The Mercury capsule had a mass of $m = 1450$ kg and a thermal shield with area $A = 2.8$ m^2. From Eq. (10.1.2) we derive that during reentry a shield temperature of roughly $T \approx 1890$ K $= 1610$ °C occurred. These temperatures are at the limit today's heat insulations can withstand.

Example 2

If a Space Shuttle with a mass $m \approx 100{,}000$ kg and an effective stagnation point area of $A \approx 5$ m^2 would have also reentried on a ballistic trajectory, it would have been exposed to $T \approx 3680$ °C and hence would have not survived, as the thermal tiles at the nose and at the front edge of the Shuttle wings were designed for a maximum of 1750 °C. Actually, the Shuttle with its high lift reduced the peak heat load by drastically extending the path through the atmosphere and thus spreading the heat over a much longer period of time about 10 min (equals blackout time, see Sect. 10.7.4). The so-called angle of attack (see Sect. 6.2.5) also displaced part of the generated heat to the lower side, which we will account for by increasing the effective stagnation point area by the factor of 2. According to Eq. (10.1.2) these measures reduced the peak temperature to $T \approx 1600$ °C. This is a conservative estimate. In fact, the measured maximal reentry temperatures at the critical wing leading edge did not exceed 1400 °C.

Heat Flux Models

These results are only rough estimates. To get more accurate results, we have to calculate the time-dependent heat flux as well as its maximum. The total heat flow rate generated by the air impinging with velocity v and mass flow rate $\dot{m} = \rho vA$ (see continuity Eq. (1.2.8)) is given by Newtonian flow theory (see Sect. 6.2.2), which holds in the free molecular flow regime at extremely low flow densities or at hypersonic speeds when the shock layer is so thin that it practically coincides with the body surface, as $\dot{Q}_{tot} = \dot{m}h_{tot}$. The total heat flux therefore is

$$\dot{q}_{tot} = \frac{\dot{Q}_{tot}}{A} = \frac{\dot{m} h_{tot}}{A} = \frac{\rho v A}{A} \frac{v^2}{2} = \frac{1}{2} \rho v^3$$

where h_{tot} is the total enthalpy per unit mass of the free streaming air, which at hypersonic speeds essentially equals the specific kinetic energy of the air flow. The portion that by diffusion mechanisms is transferred to the S/C is

$$\dot{q}_{S/C} = St \cdot \dot{q}_{tot} = \frac{St}{2} \rho v^3$$

This is the elementary theoretical result for the heat flux of a flat plate with area A.

The more sophisticated and most common one-dimensional, steady, inviscid, adiabatic flow theory of dissociating gas in thermochemical equilibrium was shown by Fay and Riddell to result in a stagnation-point heat transfer rate equation, so-called *Fay–Riddell equation* (Bertin 1994, Eq. 5-36), which for a cold wall approximation reads (Bertin 1994; Hirschel 2004)

$$\begin{aligned} \dot{q}_{S/C} &= \frac{St}{2} \sqrt{\rho \rho_q \frac{R_0}{R_n}} \cdot v^3 \\ &= \dot{q}_e \sqrt{\frac{\rho}{\rho_e} \frac{R_0}{R_n}} \cdot \left(\frac{v}{v_\triangleright} \right)^3 \end{aligned} \tag{10.1.3}$$

with

$$\begin{aligned} &\rho_q = 0.121 \text{ kg m}^{-3} = 0.121 \text{ W s}^3 \text{ m}^{-5} \quad @ \ St = 1.00 \times 10^{-3} \\ &\rho_e = 1.80 \times 10^{-8} \text{ kg m}^{-3} \\ &R_0 = 1 \text{ m} \\ &v_\triangleright = 7.905 \text{ km s}^{-1} \text{ first cosmic velocity} \\ &\dot{q}_e = \frac{St}{2} \sqrt{\rho_q \rho_e} \cdot v_\triangleright^3 = 1.15 \text{ W cm}^{-2} \end{aligned}$$

where ρ_q corresponds to the so-called Sutton-Graves value of the stagnation point heat transfer coefficient, ρ_e is the mean atmospheric density at entry interface according to MSIS-E-90, R_n the radius of the surface curvature at that (nose) point where stagnation occurs, and $\dot{q}_e$ the standard heat flux at entry interface.

According to highly sophisticated one-dimensional adiabatic steady-state heat flux models the heat flux at the stagnation points of an aeroshell at hypersonic speeds was generally determined to be $\dot{q}_{S/C} \propto \sqrt{\rho / R_n} \cdot v^x$ with $x = 3.00 - 3.22$ depending on details of the model with $x = 3$ if the viscosity of the medium is proportional to $\sqrt{T}$. Because it can be shown that the essential results of this chapter vary at maximum by 1% depending on x, we assume in the following the Fay–Riddell equation with $x = 3$.

Example

Upon reentry of the Space Shuttle through Earth's atmosphere the maximum stagnation point heating occured at 68.9 km altitude, where $\rho = 1.075 \times 10^{-4}$ kg m^{-3} and $v = 6.61$ km s^{-1}. At that trajectory point the Shuttle had a 40° angle of attack, which brings about an effective nose radius of 1.29 m. What is the stagnation point heat flux?

According to Eq. (10.1.3) we find $\dot{q}_{S/C} = 45.7$ W cm^{-2}. Based on experimental data from the Space Shuttle, Zoby (1982) quotes a maximum stagnation point heat flux of $\dot{q}_{S/C} = 45$ W cm^{-2}, very close to our result.

At a given entry velocity profile $v = v(\rho)$ this heat flux at the stagnation point achieves its maximum for $d\dot{q}/d\rho = 0$. This is the conditional equation, which we will use in this chapter to calculate the peak heat flux, which in turn can be inserted into Eq. (10.1.1) to derive the peak surface temperature of the S/C.

10.1.2 Entry Interface

Let us have a closer look at the reentry process into the atmosphere. Reentry formally commences at the so-called entry interface.

> According to international agreements, the entry interface is located at an altitude of 400,000 ft = 122 km, i.e., at the border between heterosphere and homosphere.

The atmosphere of course does not abruptly set in at this altitude, but drag and lift start there to have an influence on the entering vehicle. According to Eq. (6.1.5) the homosphere below 120 km the atmospheric density obeys the barometric formula

$$\rho(r) = \rho_0 \exp\left(-\frac{r-R}{H}\right) = \rho_0 \exp\left(-\frac{h}{H}\right)$$

with $\rho_0 = 1.752$ kg/m^3 and $H = 6.7 \pm 0.1$ km average scale height for the entire homosphere.

At the entry interface the orbit parameters take on the values r_e, v_e, γ_e. According to standard conventions (for details see Sect. 10.2) the flight path angle γ of a reentry vehicle (a.k.a. *entry angle* or *velocity angle*) is to be understood as a positive angle, and hence also $\gamma_e > 0$.

10.1.3 Deorbit Phase

Before we study the reentry into the atmosphere it needs to be known how the S/C gets from its preceding trajectory to the entry interface. Usually the starting point is a circular Earth orbit, the radius of which we denote by r_i (initial). Deorbit is initiated by a deorbit burn at a certain position on this orbit, which transfers the S/C onto an entry ellipse with a low-lying periapsis, which intersects the entry interface at a predetermined flight path angle γ_e (see Fig. 10.2). The deburn position has to be chosen such that the entry point is at the right distance to the anticipated landing site. We now want to evaluate the questions: What is the required delta-v for the deorbit? At which position is the entry interface attained? What is the entry velocity at entry interface? It is now our objective to determine these three values.

At deorbit burn the S/C is positioned at the apoapsis of the entry ellipse with the still to be determined orbital elements a, e. If this ellipse is supposed to intersect the entry interface at position r_e, θ_e with entry velocity v_e the ellipse is unequivocally determined because Eqs. (7.3.16b), (7.3.14), and (7.3.5), state that the following holds:

$$\begin{aligned} \cos\gamma_e &= \frac{1+e\cos\theta_e}{\sqrt{1+2e\cos\theta_e+e^2}} \\ v_e &= \frac{\mu}{h}\sqrt{1+2e\cos\theta_e+e^2} \\ r_e &= \frac{a(1-e^2)}{1+e\cos\theta_e} = R+h_e = 6500\ \text{km} \end{aligned} \tag{10.1.4}$$

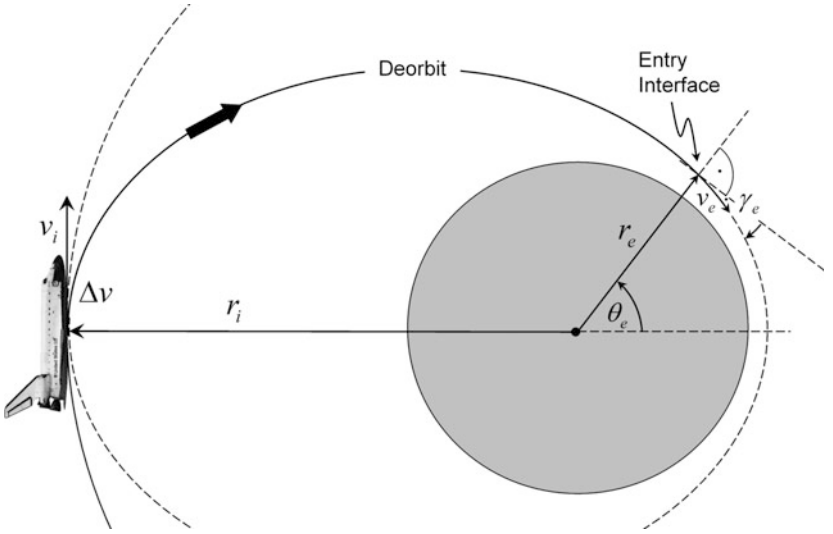

Fig. 10.2 Deorbit phase: from deorbit burn to entry interface

The orbital elements are not independent from each other because we have at the deorbit position at apogee

$$r_i = a(1+e) \tag{10.1.5}$$

From this condition and from Eq. (10.1.4) we derive

$$e\cos\theta_e = \frac{a(1-e^2)}{r_e} - 1 = \alpha(1-e) - 1 \tag{10.1.6}$$

with

$$\alpha := \frac{r_i}{r_e} = \frac{r_i}{6500\ \text{km}} > 1 \tag{10.1.7}$$

and

$$h = \sqrt{\mu a(1-e^2)} = \sqrt{\mu r_i(1-e)}$$

We insert these results back into Eq. (10.1.4) and find after some trivial steps

$$\begin{aligned}
\cos\gamma_e &= \alpha\sqrt{\frac{1-e}{2\alpha-1-e}} \\
v_e &= v_i\sqrt{2\alpha-1-e} \\
e\cos\theta_e &= \alpha(1-e)-1 \\
\Delta v &= \sqrt{\frac{\mu}{r_i}} - \sqrt{\frac{\mu}{a}\frac{1-e}{1+e}} = v_i\left(1-\sqrt{1-e}\right)
\end{aligned}$$

with

$$v_i = \sqrt{\frac{\mu}{r_i}}$$

the orbital velocity of the initial orbit and Δv the propulsion demand for the deorbit burn. These equations have to be interpreted as follows. At a given r_i, r_e, γ_e the first equation delivers the eccentricity e of the entry ellipse. With this we find from the other equations the wanted entry velocity and the propulsion demand for deorbit. This is exactly what we are going to do now. From the first equation we derive after some rearrangements

$$e = \frac{\alpha^2 - (2\alpha-1)\cos^2\gamma_e}{\alpha^2 - \cos^2\gamma_e} \tag{10.1.8}$$

We insert this into the other three equations and find

$$v_e = \alpha v_i \sqrt{\frac{2\alpha_-}{\alpha^2 - \cos^2\gamma_e}} = \sqrt{\frac{2\mu}{r_e}\frac{\alpha\alpha_-}{\alpha^2 - \cos^2\gamma_e}} \tag{10.1.9a}$$

$$\Delta v = v_i\left(1 - \cos\gamma_e\sqrt{\frac{2\alpha_-}{\alpha^2 - \cos^2\gamma_e}}\right) = v_i - \frac{\cos\gamma_e}{\alpha}v_e \tag{10.1.9b}$$

$$\cos\theta_e = \frac{\alpha_-^2\cos^2\gamma_e - \alpha^2\sin^2\gamma_e}{\alpha_-^2 + \alpha^2\sin^2\gamma_e} \tag{10.1.9c}$$

with $\alpha := \frac{r_i}{r_e} = \frac{r_i}{6500\text{ km}}, \alpha_- := \alpha - 1 = \frac{r_i}{r_e} - 1, v_i = \sqrt{\frac{\mu}{r_i}}$

These are the wanted expressions. There are only two cases of practical interest: $\alpha \approx 1$ and $\alpha \to \infty$, which we will investigate now.

Interplanetary Reentry ($\alpha \to \infty$)
The S/C approaches Earth from infinity, for instance from the Moon or from a planet, for aerocapture and subsequent reentry. In this case we simply get

$$\begin{aligned} v_e &\approx \sqrt{\tfrac{2\mu}{r_e}\left(1 - \tfrac{1}{\alpha}\right)} \approx \sqrt{\tfrac{2\mu}{r_e}} \\ \Delta v &\approx v_i\left(1 - \cos\gamma_e\sqrt{\tfrac{2}{\alpha}}\right) \approx v_i \approx 0 \quad @\ \ \gamma_e^2 \ll 1 \\ \theta_e &= 2\gamma_e \end{aligned} \tag{10.1.10}$$

As expected, the entry velocity is the second cosmic velocity (see Sect. 7.4.4), and the deorbit burn effort becomes arbitrarily small. Of course the burn cannot be performed so precisely as to hit exactly the entry interface. Therefore, the entry trajectory usually must be adjusted several times during approach to pass through the so-called entry corridor to ensure aerocapture (see also Sect. 10.5.2). Figure 10.3 displays the entry corridor for Apollo 11. Three adjusting maneuvers were planned for this Moon mission to enter the corridor.

LEO Reentry ($\alpha \to 1$)
The S/C initially is in a LEO. For $\gamma_e \leq 10°$ the trigonometric functions can be approximated and because then $\gamma_e^4 \ll 20 \cdot \alpha_-$, Eqs. (10.1.9a) and (10.1.9b) can be written as (exercise, Problem 10.1)

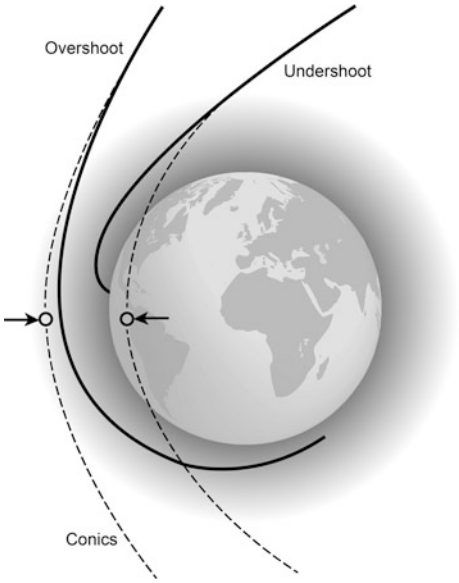

Fig. 10.3 Limiting trajectories of the Apollo reentry corridor

$$\begin{aligned} v_e &= v_i\left(1+\tfrac{3}{4}\alpha_- - \frac{\gamma_e^2}{8\alpha_-}\right) \\ \Delta v &= \tfrac{v_i}{4}\left[\alpha_- + \frac{\gamma_e^2}{2\alpha_-}\right] \end{aligned} \quad @ \quad \gamma_e \le 10^\circ \qquad (10.1.11)$$

from which follows

$$\begin{aligned} v_e < v_i \quad @ \quad \gamma_e > \sqrt{6}\cdot\alpha_- \\ v_e > v_i \quad @ \quad \gamma_e < \sqrt{6}\cdot\alpha_- \end{aligned}$$

For θ_e no simpler expression can be derived than that in Eq. (10.1.9c).

Example

After undocking from the ISS at 400 km altitude ($\alpha = 1.0428, v_i = 7.669$ km s^{-1}) the Space Shuttle had to deorbit such that it encounters the entry interface with a standard flight path angle $\gamma_e = 1^\circ$. According to Eqs. (10.1.9c) and (10.1.11) we obtain: $\theta_e = 46.1^\circ, v_e = 1.031 \cdot v_i = 7.91$ km s^{-1}, and $\Delta v = 0.0116 \cdot v_i = 88.8$ m s^{-1} (cf. Shuttle Reentry, Sect. 10.7.1).

On the other hand the Soyuz capsule after undocking from the ISS usually acquires a flight path angle of $\gamma_e = 3^\circ$ at entry interface. We find from Eqs. (10.1.9c) and (10.1.11): $\theta_e = 76.2^\circ, v_e = 1.024 \cdot v_i = 7.85$ km s^{-1}, and $\Delta v = 0.0187 \cdot v_i = 143$ m s^{-1}.

Note *For all flat entries from LEO the entry velocity is* $v_e \approx v_\triangleright$, *where* $v_\triangleright = \sqrt{g_0 R_\oplus} = 7.905\ \mathrm{km\ s^{-1}}$ *is the first cosmic velocity, while for entries from infinity (celestial bodies)* $v_e \approx v_{\triangleright\triangleright}$ *with* $v_{\triangleright\triangleright} = \sqrt{2 g_0 R_\oplus} = 11.18\ \mathrm{km\ s^{-1}}$ *the second cosmic velocity. Therefore, the assumptions, which we are going to be used in the following reentry investigations,* $\varepsilon_e = v_e^2/v_\triangleright^2 = 1$ *and* $\varepsilon_e = v_e^2/v_\triangleright^2 = 2$, *respectively, are excellent assumptions for these two cases.*

10.2 Equations of Motion

We are now at entry interface, where atmospheric reentry commences. As reentry is subject to the same physical laws as ascent, we adopt the general orbit Eqs. (6.3.6)–(6.3.12). But in contrast to ascent, no propulsion is required, and this is why we set thrust and also the mass change rate $\dot{m} = 0$ to zero.

According to our current definition a descending S/C would have negative flight path angle. But to be in line with standard conventions it should be positive (see Fig. 10.4). So we formally apply the transformation $\gamma \to -\gamma$, and $\dot{\gamma} \to -\dot{\gamma}$ to Eqs. (6.3.6)–(6.3.12), which results in

$$\dot{v} = -\frac{D}{m} + g \sin\gamma \tag{10.2.1}$$

$$v\dot{\gamma} = -\frac{L}{m} + \left(g - \frac{v^2}{r}\right)\cos\gamma \tag{10.2.2}$$

$$\begin{aligned} \dot{h} &= -v \sin\gamma \\ \dot{x} &= v \cos\gamma \end{aligned} \tag{10.2.3}$$

with altitude $h = r - R$, radius of the planet R, downrange distance x, and (see Sects. 6.2.3 and 7.1.2)

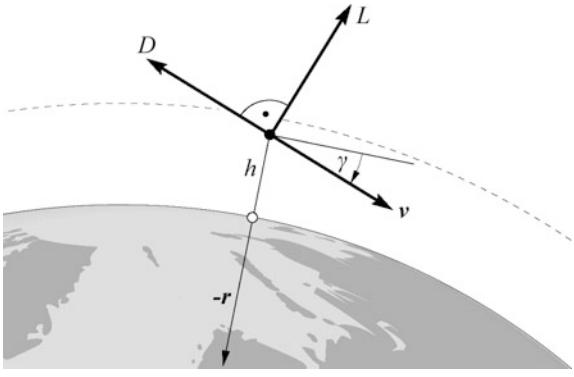

Fig. 10.4 Definition of the reentry variables

$$D = \frac{1}{2}\rho(r)v^2 C_D A_\perp = mv^2 \frac{\kappa_D}{H} e^{-\frac{h}{H}} \tag{10.2.4}$$

$$L = \frac{1}{2}\rho(r)v^2 C_L A_\perp = mv^2 \frac{\kappa_L}{H} e^{-\frac{h}{H}} \tag{10.2.5}$$

$$g(r) = g_0 \frac{R^2}{r^2} \tag{10.2.6}$$

We recall from Sect. 6.3 that we assume lift forces to lie in the motion plane and the S/C therefore remains in this plane and we have no cross motion.

10.2.1 Normalized Equations of Motion

To study the behavior of reentry we need to solve the equations of motion numerically in their time-dependent representation. Because Eqs. (10.2.1)–(10.2.3) are afflicted by physical dimensions, they are not suitable for that. We therefore revert to the dimensionless form of the equations of motion as given by Eq. (6.3.13). For reentry we set the normalized thrust $\Phi = 0$ and again apply the formal transformation $\gamma \to -\gamma$, and $\dot{\gamma} \to -\dot{\gamma}$, thus getting the following result

$$\boxed{\begin{aligned} \mu' &= -\mu^2 \kappa_D \frac{R}{H} e^{-\eta} + \sin\gamma \\ \mu\gamma' &= -\mu^2 \kappa_D \frac{R}{H}\frac{L}{D} e^{-\eta} + (1-\mu^2)\cos\gamma \\ \eta' &= -\mu \sin\gamma \\ \chi' &= \mu \cos\gamma \end{aligned}} \tag{10.2.7}$$

with

$$\boxed{\begin{aligned} &\mu = \frac{v}{v_\triangleright}, \eta = \frac{h}{H}, \chi = \frac{x}{H} \\ &\tau = \frac{g_0}{v_\triangleright} t, \ (\ldots)' = \frac{d}{d\tau}, \\ &v_\triangleright = \sqrt{g_0 R} \end{aligned}}$$

We recall that the first three equations are coupled, and that η', χ' are the normalized altitude and downrange velocities, respectively, which enable us to derive the time-dependent solutions $h(t), x(t)$ and hence the ascent and reentry trajectory $h = h(x)$. The equations of motion in form of Eq. (10.2.7) are optimally adapted to be coded and solved numerically such as by a Runge-Kutta method. For specific problems more elaborate equations without the approximations made here (see beginning of Sect. 10.3) are used. The relatively simple equations above however capture general entry behavior, so we will limit ourselves to them.

Significance of *L/D* Ratio

Equations (10.2.7) make clear that there is only one characteristic S/C variable, L/D, to control the reentry trajectory. We recall from Sect. 6.2.5 that for hypersonic velocities L/D largely depends on the angle of attack (AOA) α. For Apollo capsules we had (see Eq. 6.2.26)

$$\frac{L}{D} = 0.0143 \cdot \alpha[^\circ] \quad @ \text{ Apollo capsule, } \alpha = 0 - 40^\circ \tag{10.2.8}$$

In the following we will assume $\alpha = 20^\circ$ and hence $L/D_{capsule} = 0.32$ (Apollo 4: L/D = 0.369). For winged bodies L/D was given in Eq. (6.2.28) as

$$\frac{L}{D} = \frac{\sin\alpha \sin 2\alpha}{2\sin^3\alpha + C_f} \quad @ \text{ winged body} \tag{10.2.9}$$

where C_f is the skin friction drag coefficient. Specifically for the Space Shuttle we found

$$C_f = 0.021\left(\frac{\rho_0 v_0}{\rho v}\right)^{1/5}, \qquad \rho_0 v_0 = 1.2041 \text{ kg m}^{-3}\, Ma \quad v \geq 3\, Ma \tag{10.2.10}$$

For the typical AOA $\alpha = 20^\circ - 42^\circ$ of a Shuttle reentry we therefore get $L/D_{Shuttle} = 1.0 - 1.8$. An average $L/D_{Shuttle,ave} = 1.3$, which we will use occasionally in the following, is therefore attained at $\alpha = 35^\circ$.

As the horizontal lift and hence the bank angle (see Sect. 6.2.5) controls the out of flight plane motion, we summarize by stating that

> The L/D ratio and hence the angle-of-attack α is the only and hence crucial parameter in controlling the powerless reentry trajectory in the flight plane, while the bank angle μ is the only control parameter for out of flight plane motion (cross-range capability).

Numerical Solutions

To get a first overview of the entry behavior, Figs. 10.5, 10.6 and 10.7, with reentry trajectories in the upper part, describe the reentry of a capsule with a typical $L/D = 0.3$ for three different entry angles: a steep $\gamma_e = 45^\circ$, a medium $\gamma_e = 10^\circ$, and a very flat entry with $\gamma_e = 2^\circ$. They were calculated with a step-size controlled Runge-Kutta method solving the above normalized system of equations. The two illustrations on the same page belong to the same entry angle. The time-dependent velocities, altitudes, and decelerations are shown in the lower illustrations. The different entry profiles as a function of the entry angle first attracts attention. Note the quite different scales of the downrange x-axes, so visually the depicted entry angles are not to scale. Only in Fig. 10.5a the x- and y-scales are the same, so the depicted profiles have accurate contours.

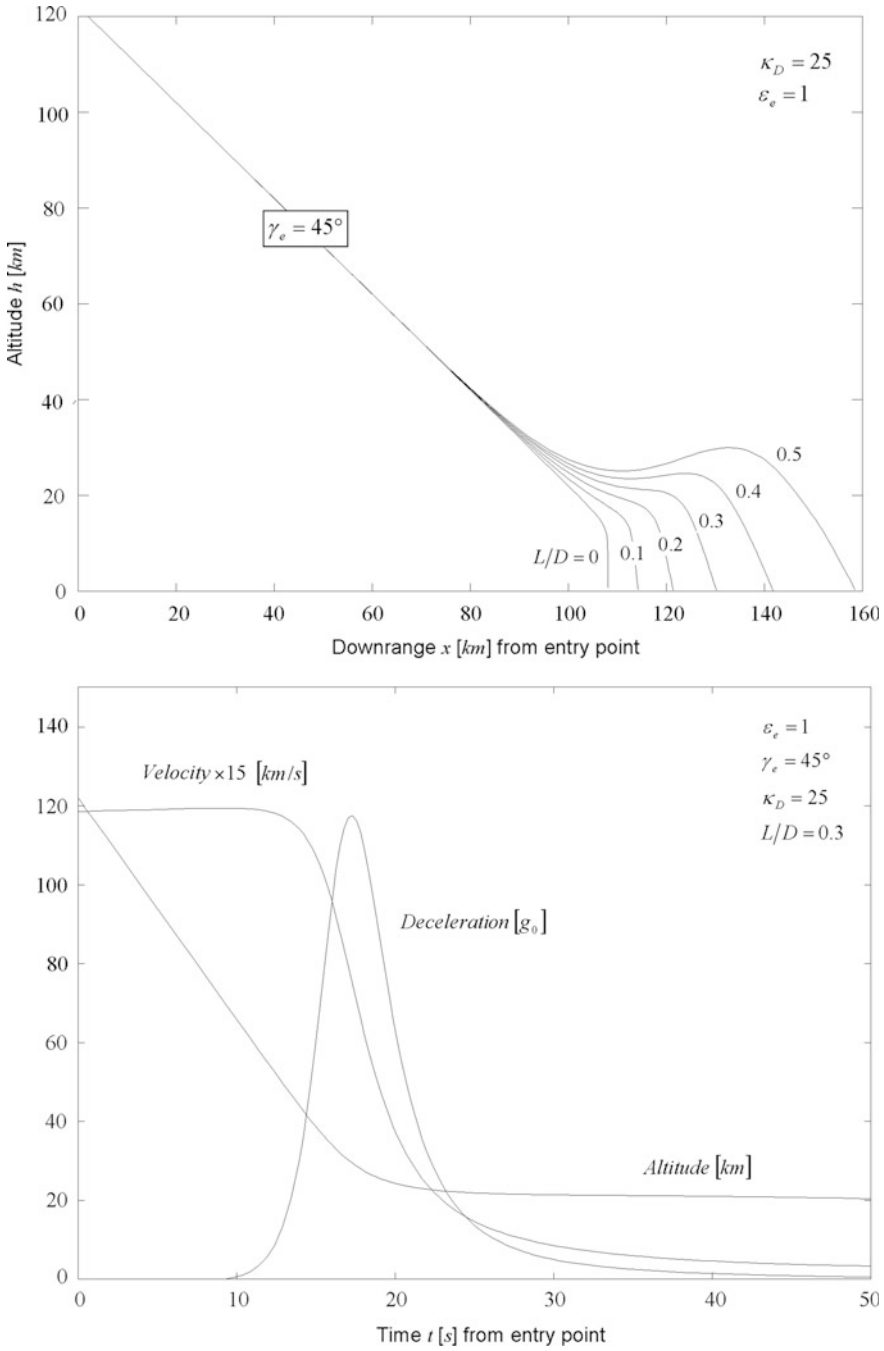

Fig. 10.5 Entry profiles of a spacecraft with $\gamma_e = 45°$

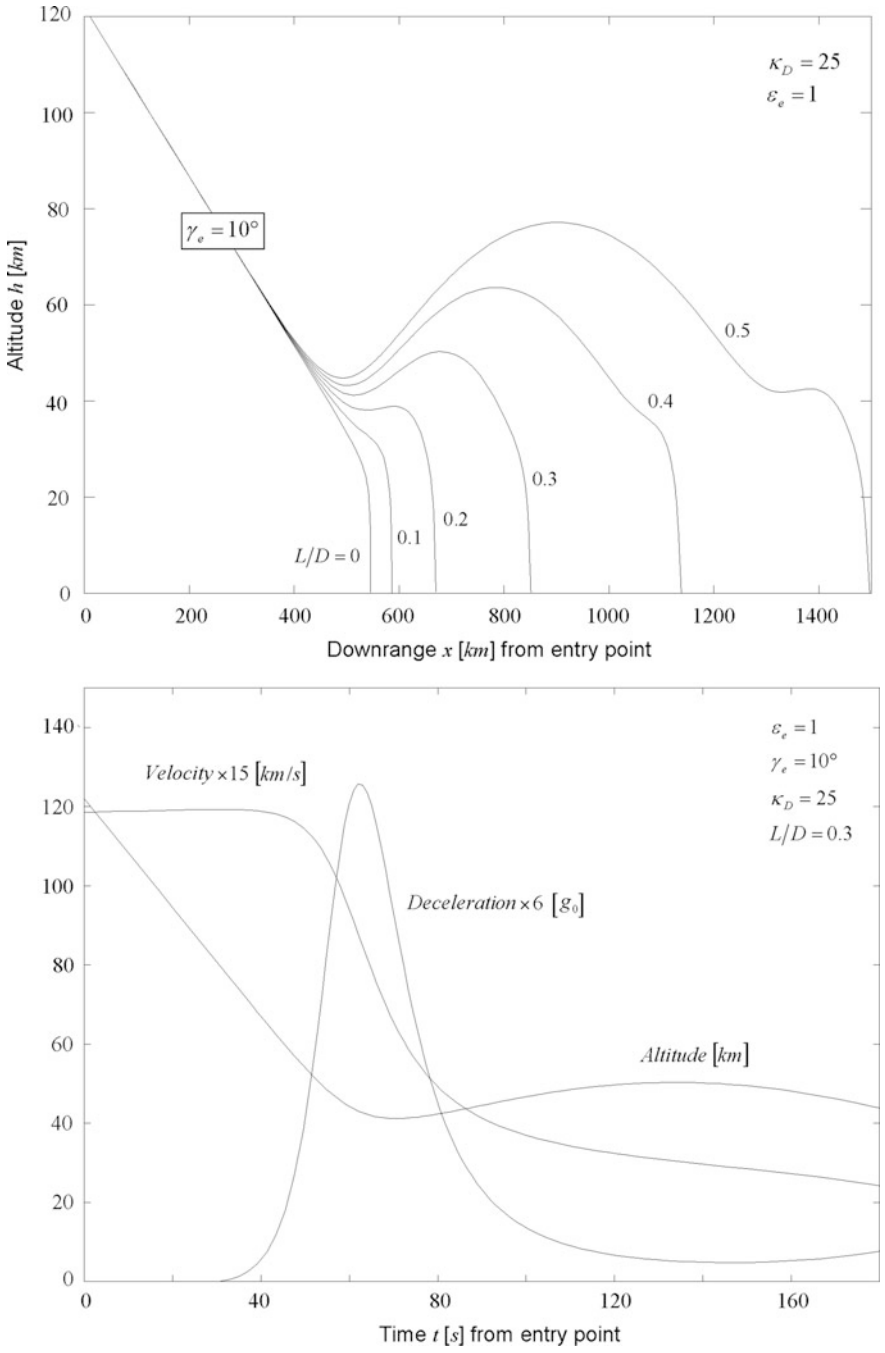

Fig. 10.6 Entry profiles of a spacecraft with $\gamma_e = 10°$

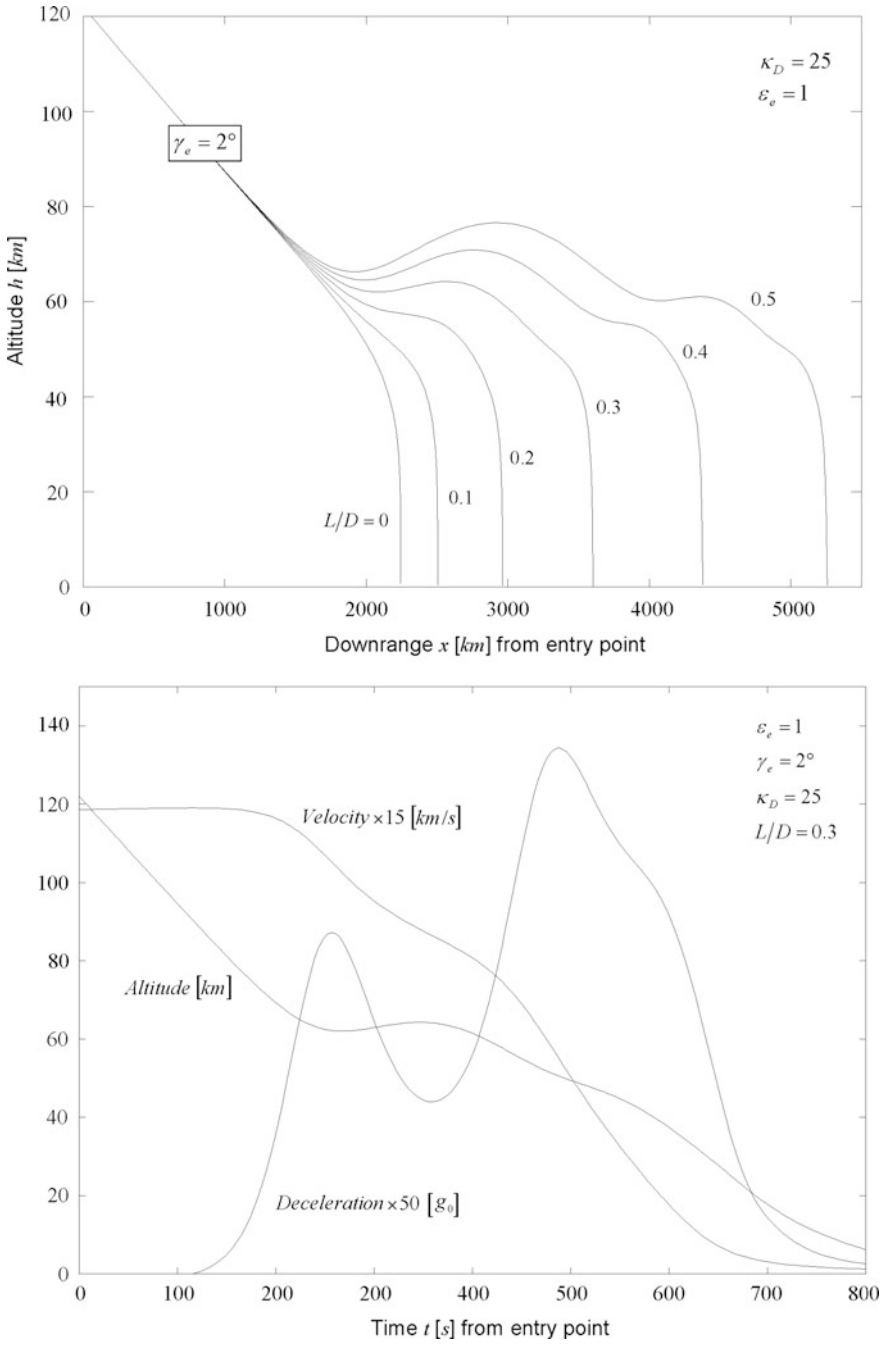

Fig. 10.7 Entry profiles of a spacecraft with $\gamma_e = 2°$

The most serious effect of flat entry angles are the increasing ranges and entry durations: A S/C with $\gamma_e = 45°$ hits the ground only 150 km downrange of the entry point, with $\gamma_e = 10°$ this comes to approximately 1000 km, and with $\gamma_e = 2°$ approximately 4000 km with correspondingly increased entry durations. Apart from that the entry profiles are the same at the beginning: With an altitude of down to 60 km, with steeper ones even down to 40 km, the reentering body moves on a straight line. Only then do lifting forces become significant. Lifts with $L/D > 0.2$ have dramatic consequences: Instead of going down continuously, the S/C literally rebounds off the atmosphere, falls back, dips in again, and then for big lifts and very flat entries slightly rises again, until it completely goes down. If the excursions are small, they are called "reflections" and "skips" for larger excursions with a subsequent ballistic coast phase. They are typical for common capsules with $L/D \approx 0.3$, and they are very pronounced for winged bodies $L/D > 1$ if there are no countermeasures. These effects, which are of quite practical interest, will be treated in detail in Sect. 10.5. Winged bodies with their more fragile structures should not enter with an angle that is too steep, because the decelerations already attain 20 g at 10°. Neither the crew nor the system would be able to endure that. These winged bodies have to enter with a very flat angle with typically 2° (Fig. 10.7), so that during the second reflection they only have to endure a maximum deceleration of merely 3 g, which is tolerable. The reason for the reduction of the deceleration is that the reduction of the velocity, i.e., the acceleration, is spread over a longer period of time, and thus it is reduced at any point in time. The critical decelerations with steeper entries $\gamma_e \geq 10°$ are always just before the reflection, and they drastically increase with an increasing entry angle. For $\gamma_e = 45°$ and $L/D = 0.3$ it already amounts to 118 g!

10.2.2 Reduced Equations of Motion

Numerical solutions are imperative for real missions, but they furnish no insight into why the entry profiles are as they are. For our goal of understanding, we need to find solutions or at least partial solutions, which mathematically relate entry parameters and entry trajectory and thus show up the limits of applicability. The above dimensionless equations of motion are still too complicated for analytical solutions, so we are looking for simplifications.

ε and γ Equations

The third differential equation relates the altitude with time. This relation allows us to substitute the time variable by the altitude variable. Thereby we get rid of the time dependence of the entry trajectory and obtain the entry variables as a function of altitude $v(h), \gamma(h)$. This is exactly what we want. So we are looking for differential equations with h as the independent variable. We again make use of Eqs. (10.2.4) and (10.2.5); this time however we substitute the entry velocity by the new dimensionless variable

$$\varepsilon := \frac{v^2}{v_\triangleright^2} = \frac{E_{kin}(v)}{E_{kin,0}}. \tag{10.2.11}$$

with $v_\triangleright = \sqrt{g_0 R_\oplus} = 7.905$ km s^{-1} which is the first cosmic velocity (see Eq. (7.4.4)). We are now set to replace the time variable t by the altitude variable. We do so by introducing the *dimensionless altitude variable* λ, which quite naturally occurs in the differential equations

$$\lambda := \frac{2\kappa_D}{\sin\gamma_e} e^{-\frac{h}{H}} = \frac{BH}{\sin\gamma_e}\rho \tag{10.2.12}$$

This altogether allows us (exercise, Problem 10.3) to transform the equations of motion into the following dimensionless form of only two coupled differential equations

$$\frac{d(\ln\varepsilon)}{d\lambda} = \underbrace{-\frac{\sin\gamma_e}{\sin\gamma}}_{drag} \underbrace{+\frac{2H}{\varepsilon\lambda R}}_{gravity} \quad \textbf{ε equation} \tag{10.2.13a}$$

$$\frac{d(\cos\gamma)}{d\lambda} = \underbrace{\frac{\sin\gamma_e}{2}\frac{L}{D}}_{lift} \underbrace{-\left(\frac{1}{\varepsilon}-1\right)\frac{H\cos\gamma}{\lambda R}}_{gravity-centrifugal} \quad \textbf{γ equation} \tag{10.2.13b}$$

Let us have a closer look at these equations. They describe the state changes of the entry body (velocity, equals kinetic energy ε, and flight path angle γ) as a function of the instantaneous altitude λ. If we compare them with Eqs. (10.2.1) and (10.2.2) we see the following. On the right-hand side of Eq. (10.2.13a) the first term is the modified drag term, and the second term is the modified gravitational term. On the right-hand side of Eq. (10.2.13b) we have the modified lift term as the first term, and the gravitational term ($1/\varepsilon$) as the second reduced by the centrifugal force (-1), the so-called *reduced gravitational term*. To be able to distinguish between the two equations later, we call the first one ε *equation* and the second one γ *equation*.

Observe that in line with Eqs. (10.2.7) the lift-to-drag ratio L/D turns out to be the only S/C variable to control the reentry trajectory.

Deceleration

Equations (10.2.13) permit to directly derive the deceleration, which is an important figure for crew and vehicle structure. By considering $\dot{h} = -v\sin\gamma$ from Eq. (10.2.3) we get

$$a = \frac{dv}{dt} = \frac{1}{d(\ln \varepsilon)/dv} \frac{d(\ln \varepsilon)}{d\lambda} \frac{d\lambda}{dh} \frac{dh}{dt} = \frac{\varepsilon v_0^2}{2v} \left[-\frac{\sin \gamma_e}{\sin \gamma} + \frac{2H}{\varepsilon \lambda R} \right] \left(-\frac{\lambda}{H} \right) (-v \sin \gamma)$$

from which because of $v^2 = \varepsilon v_\triangleright^2 = \varepsilon g_0 R$ follows

$$a = -\frac{v^2 \lambda}{2H} \sin \gamma_e + g_0 \sin \gamma = -g_0 \left(\frac{\varepsilon \lambda R}{2H} \sin \gamma_e - \sin \gamma \right) \tag{10.2.14}$$

So, except a short period of time after entry (drag-free phase, see Sect. 10.3.1), when the S/C accelerates due to gravitation and negligible drag ($\lambda \ll R/H$), the expression in the brackets is positive and the vehicle decelerates. Once we have determined the entry profiles $v(h)$ and $\gamma(h)$ for any reentry case by solving the ε and γ equations, Eq. (10.2.14) will provide us the answer to the crucial question: "What is the deceleration and in particular the maximum and hence critical deceleration a_{crit} of the spacecraft and hence also for the crew?"

Chapman's Theory

There exist other and even more sophisticated transformations to simplify the equations of motion, most notably by Chapman (1959, see also Vinh et al. 1980). He defines the normalized horizontal speed as the independent variable

$$\bar{u} := \frac{v}{v_\triangleright} \cos \gamma \quad \text{independent variable}$$

and

$$Z := \frac{1}{2} \lambda \bar{u} \sin \gamma_e \sqrt{\frac{R}{H}} \quad \text{dependent variable}$$

This yields a single second-order differential equation of motion

$$\bar{u} \frac{d}{d\bar{u}} \left(\frac{dZ}{d\bar{u}} - \frac{Z}{\bar{u}} \right) = \frac{1 - \bar{u}^2}{\bar{u} Z} \cos^4 \gamma - \sqrt{\frac{R}{H}} \frac{L}{D} \cos^3 \gamma$$

Chapman (1961) (see also Vinh et al. 1980) published the expression $\bar{u} \cdot Z(\bar{u})$ as a function of $\bar{u}$ for various entry profiles $\gamma_e, L/D$. Note that

$$\bar{u} \cdot Z(\bar{u}) = \frac{a \cdot \cos^2 \gamma}{\sqrt{1 - (L/D)^2}} \sqrt{\frac{H}{R}}$$

So, Chapman's theory essentially provides the acceleration a at a given velocity, but gives no insight into the reentry trajectory $\gamma(h)$ and velocity profile $v(h)$. In the following reentry analysis we therefore stick to the ε and γ equations as given by Eqs. (10.2.13a) and (10.2.13b), which provides these two revealing reentry profiles.

10.3 Elementary Results

From the above numerical solutions of the complex entry profiles it is evident, that there are no global analytical solutions. We will therefore focus on certain entry phases, which allow approximate analytical solutions, in particular in the critical deceleration phase.

General Approximations
To do so we have to make some gentle approximations to simplify the equations:

- Gravitation $g = g_0 = const.$
  According to Eq. (10.2.6), this assumption entails an error of $(6370/6248)^2 \leq 4.0\%$. If one chooses for g the mean value of $\langle g \rangle_h = 9.62$ m/s^2 at an altitude of 61 km, the error is even reduced to $(6370/6309)^2 \leq 2.0\%$.
- $v^2/r \approx v^2/R \approx v^2/r_e$
  This assumption entails an error of $6370/6248 \leq 2.0\%$.
- κ_D is assumed to be constant during the whole reentry process.
  The actual deviations from this constant for a S/C with a constant angle of attack are no more than $\pm 10\%$. If the angle of attack slightly changes, the important parameter L/D is still within a $\pm 10\%$ range.

The first two errors are negligible with regard to the third assumption, to all prior assumptions (e.g., a constant scale height for the barometric Formula (6.1.5), to the assumption that the Earth is a non-rotating inertial system), and other qualitative assumptions we will make later on.

10.3.1 Drag-Free Phase

The S/C is now at the entry interface at 122 km altitude with state vector (r_e, γ_e). Reentry can be roughly divided into two different phases as illustrated in Fig. 10.8.

Directly after entry, the aerodynamic drag is so low that drag can practically be neglected. So the body descends with the entry angle almost in free fall toward Earth. The motion Eqs. (10.2.1)–(10.2.3) therefore and because of $v^2 \approx gR^2/r \approx gr$ (circular orbital velocity) reduce to

$$\begin{aligned} \dot{v} &\approx g \sin\gamma \\ \dot{\gamma} &\approx 0 \\ \dot{h} &= -v \sin\gamma \end{aligned}$$

in this reentry phase. Integration results in

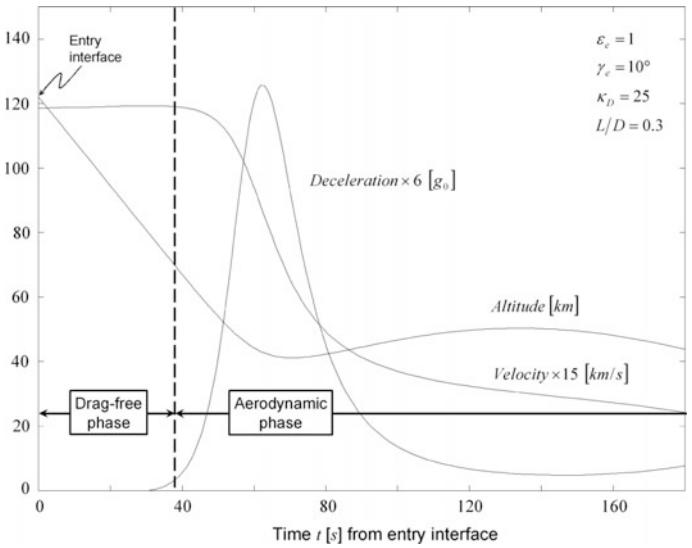

Fig. 10.8 The onset of deceleration departs the aerodynamic phase from the drag-free phase

$$\begin{aligned} \gamma &= \gamma_e \\ v &= v_e + g \sin\gamma_e \cdot t \approx const \\ h &= h_e - v_e \sin\gamma_e \cdot t \end{aligned} \tag{10.3.1}$$

This is exactly the behavior we observe also in the numerical results in Figs. 10.4, 10.5 and 10.6. As v_e is still very big, altitude decreases strongly while the velocity increases only slightly.

Note *The reason for the absolutely straight reentry trajectory, rather than one which is bent downward due to gravity as one might expect, is the centrifugal force, which like in a circular orbit still counterbalances the gravitational force.*

Below approximately 70–80 km, the impinging air behaves like a free molecular flow with a rapidly increasing aerodynamic drag. This is where the crucial aerodynamic phase starts. The transition between the two phases takes place when $d\varepsilon/d\lambda = 0$ and is characterized by the onset of a deceleration. According to Eq. (10.2.13a), this implies that

$$\frac{\sin\gamma_e}{\sin\gamma} = \frac{2H}{\varepsilon\lambda R}$$

Because of Eq. (10.2.12), $\varepsilon \approx 1$, and $\gamma \approx \gamma_e$, this determines the altitude of transition between the two phases to be

$$h_{trans} = H \ln\left(\frac{\kappa_D R}{\sin\gamma_e H}\right) \tag{10.3.2}$$

It mainly depends on γ_e and reaches for flat entries, $\gamma_e = 2^\circ - 10^\circ, h_{trans} = 85 - 95$ km, and for steep entries, $\gamma_e = 10^\circ - 45^\circ, h_{trans} = 75 - 85$ km (cf. Figs. 10.5, 10.6 and 10.7). Observe that the condition $d\varepsilon/d\lambda = 0$ marks also the maximum kinetic energy and hence velocity of the vehicle. Therefore, at the phase transition altitude h_{trans} the vehicle acquires its peak reentry velocity.

Adjusted Scale Height
Because the decisive action of the following reentry happens in the altitude range $30\text{ km} < h < 70$ km we adjust the scale height of the barometric formula for further calculations to this altitude, which is (see Table 6.2)

$$\boxed{H \approx 7.6\text{ km}} \quad @ \quad 30\text{ km} < h < 70\text{ km} \tag{10.3.3}$$

or we will later adjust it to the particular altitude under consideration.

10.3.2 Ballistic Reentry

The above numerical calculations show that the entry profiles in the aerodynamic phase may be quite different and complex. So it would be foolish to tackle the equations of motion head on. First of all, we need to understand the basic behavior of the solutions without the perturbing gravitation and lift terms L/D and H/R. This determines our approach, step by step, from simple approximations of equations to the more difficult ones. So we start out by neglecting the perturbation terms L/D and H/R to find solutions for a non-disturbed reentry, and later, we will also take into account lift and gravitational perturbations.

We first assume that the S/C does not have any lift, $L/D = 0$. This is the so-called *ballistic reentry*. The expression "ballistic" refers to "like the flight of a ball", which does not have any lift. Except for truly spherical reentry bodies, which do not exist in practice, $L = 0$ is only valid for axially symmetric bodies with absolutely no angle of attack (AOA, which is the angle between the axis of symmetry and oncoming flow). In reality even small AOAs produce differences in the position of the center of mass and the center of aerodynamic pressure and therefore significant lift. If this is not desired (because skipping can easily occur (see Sect. 10.5), and the resulting difficulty to determine the landing site), so if a true ballistic trajectory is wanted, one can slowly roll the S/C to average out such lifts. The Mercury capsule for instance had a nominal roll rate of 15° per second.

LEO Reentry Profile with Large Drag

For a rough result and as the second assumption we assume that compared to drag all other forces acting on the vehicle are negligible, which is true for altitudes below about 70 km (see Fig. 10.8). So setting the gravitational term to zero in Eq. (10.2.13a) and in Eq. (10.2.13b) $L = 0$ and $\varepsilon = \varepsilon_e = 1$ for an LEO reentry, the corresponding differential equations read

$$\begin{aligned} \frac{d(\ln \varepsilon)}{d\lambda} &= -\frac{\sin \gamma_e}{\sin \gamma} \\ \frac{d(\cos \gamma)}{d\lambda} &= 0 \end{aligned} \tag{10.3.4}$$

This set of equation can be solved easily. The second equation directly yields $\cos \gamma = \cos \gamma_e = const$ and therefore

$$\boxed{\gamma = \gamma_e = const} \tag{10.3.5}$$

Because the reentry body is subject just to drag, it entries on a straight line (cf. Figs. 10.5 and 10.6) and decelerates. This deceleration is described by the term on the right-hand side of the first Eq. (10.3.4). We can solve this equation as well by inserting Eq. (10.3.5)

$$\int_{e_e}^{\varepsilon} d(\ln \varepsilon') = -\int_{\lambda e}^{\lambda} d\lambda'$$

Integration delivers

$$\ln \frac{\varepsilon}{\varepsilon_e} = -(\lambda - \lambda_e)$$

and hence

$$\varepsilon = \varepsilon_e e^{-(\lambda - \lambda_e)} \approx \varepsilon_e e^{-\lambda} \tag{10.3.6}$$

The latter holds because $\lambda_e \approx 10^{-7}$. With Eq. (10.2.11) we find from Eq. (10.3.6) for the velocity

$$v = v_e e^{-(\lambda - \lambda_e/2)} \approx v_e e^{-\lambda/2} \tag{10.3.7}$$

As we will see later Eqs. (10.3.5) and (10.3.7) are useful descriptions for any early entry phase where drag exceeds lift and gravitational forces. This is why these results despite their simplicity are of general significance even for very flat lifting reentries (cf. Sect. 10.6; Eq. (10.6.4)).

General Reentry Profile

We now relax the large drag assumption to include also the pull of gravity for a ballistic reentry not only from LEO, but possibly also beyond. Gravity will firstly change the flight path angle. We therefore insert the above first-order result into Eq. (10.2.13b) for an iterative refinement and get

$$\frac{d(\cos\gamma)}{\cos\gamma} = -\frac{H}{\varepsilon_e R}\frac{e^{\lambda}-\varepsilon_e}{\lambda}d\lambda$$

Since

$$\int \frac{e^x}{x}dx = Ei(x) \approx \gamma + \ln x + x$$

where $\gamma = 0.57721\ldots$ is Euler's constant, we get

$$\ln\frac{\cos\gamma}{\cos\gamma_e} = -\frac{H}{\varepsilon_e R}\left[\lambda - (\varepsilon_e - 1)\ln\frac{\lambda}{\lambda_e}\right]$$

Because $\frac{H}{\varepsilon_e R}\left[\lambda - (\varepsilon_e - 1)\ln\frac{\lambda}{\lambda_e}\right] < 0.01$ we can approximate

$$\frac{\cos\gamma}{\cos\gamma_e} = 1 - \frac{H}{\varepsilon_e R}\left[\lambda - (\varepsilon_e - 1)\ln\frac{\lambda}{\lambda_e}\right]$$

From this follows after a short and straight forward auxiliary calculation

$$\frac{\sin\gamma}{\sin\gamma_e} = 1 + \frac{H}{\varepsilon_e R}\lambda\cot^2\gamma_e$$

We insert this result into Eq. (10.2.13a) to find

$$d(\ln\varepsilon) = -\left(1 - \frac{H}{\varepsilon_e R}\lambda\cot^2\gamma_e\right)d\lambda + \frac{2H}{\varepsilon_e R}\frac{e^{\lambda}}{\lambda}d\lambda$$

Integration and using $\varepsilon_e = v_e^2/(gR)$ from Eq. (10.2.11) delivers

$$\begin{aligned}\ln\frac{v(\lambda)}{v_e} &= \underbrace{-\frac{\lambda}{2}}_{drag} \underbrace{+\frac{gH}{v_e^2}\ln\frac{\lambda}{\lambda_e}}_{gravity} \underbrace{+\frac{gH}{v_e^2}\frac{1}{4}\lambda^2\cot^2\gamma_e}_{FPA\ change} \\ &\approx -\frac{\lambda}{2} + \frac{gH}{v_e^2}\ln\frac{\lambda}{\lambda_e}\end{aligned} \quad @\ L = 0 \tag{10.3.8}$$

where the latter follows from $\frac{1}{4}\lambda^2\cot^2\gamma_e \ll \ln\lambda/\lambda_e$ for any practical FPA. This is the more refined result of Eq. (10.3.7) of the second order.

To also find a more useful $v(t)$ rather than the above $v(\lambda)$, we need to determine $\lambda(t)$, that is $h(t)$ because according to Eq. (10.2.12)

$$\lambda := \frac{2\kappa_D}{\sin\gamma_e} e^{-\frac{h}{H}}$$

We do this by integrating $\dot{h} = -v\sin\gamma \approx -v\sin\gamma_e$ yielding with Eq. (10.3.8)

$$h - h_e = -v_e \sin\gamma_e \int_0^t \exp\left(-\frac{\lambda}{2} + \frac{gH}{v_e^2}\ln\frac{\lambda}{\lambda_e}\right) \cdot dt$$

and since the value of the expression in the exponent is less than 0.1

$$h(t) \approx h_e - v_e \sin\gamma_e \int_0^t \left(1 - \frac{\lambda}{2} + \frac{gH}{v_e^2}\ln\frac{\lambda}{\lambda_e}\right) \cdot dt \quad @\ L = 0$$

Consider this result as an equation to iteratively determine and hence improve $h(\lambda(h(t)))$. As a first iteration we assume $\lambda = \lambda_e < 10^{-5} \approx 0$ and hence find

$$h(t) \approx h_e - v_e \sin\gamma_e \cdot t$$

or equivalently

$$\frac{\lambda}{2} = \frac{\lambda_e}{2}\exp\left(\frac{v_e \sin\gamma_e}{H} t\right)$$

In a second iteration we insert this result to obtain

$$h(t) = h_e \underbrace{-v_e \sin\gamma_e \cdot t}_{\text{initial speed}} \underbrace{-\frac{1}{2} g \sin^2\gamma_e \cdot t^2}_{\text{gravity}} \underbrace{+ H\frac{\lambda_e}{2}\exp\left(\frac{v_e \sin\gamma_e}{H} t\right)}_{\text{drag}} \quad @\ L = 0 \tag{10.3.9}$$

The drag term has a positive algebraic sign because drag reduces speed. Therefore, at constant flight path angle the vehicle descents in a given time period a shorter distance than in free fall. With the definition

$$\Delta\eta(t) := \frac{h_e - h(t)}{H} = \frac{v_e}{H}\sin\gamma_e \cdot t + \frac{1}{2}\frac{g}{H}\sin^2\gamma_e \cdot t^2 - \frac{\lambda_e}{2}\exp\left(\frac{v_e \sin\gamma_e}{H} t\right)$$

Equation (10.3.9) yields $\lambda/2 = \lambda_e/2 \cdot \exp(\Delta\eta)$, which inserted into Eq. (10.3.8) finally delivers

$$\boxed{\ln\frac{v(t)}{v_e} = -\frac{\lambda_e}{2}\exp(\Delta\eta) + \frac{gH}{v_e^2}\Delta\eta} \quad @ \quad L = 0 \tag{10.3.10}$$

Critical Deceleration

According to Eq. (10.3.6) the kinetic energy decreases exponentially with λ. But because initially $\lambda \ll 1$, the velocity at the beginning of the drag-free phase decreases only slowly (see Fig. 10.8). The maximum velocity reduction, that is the maximum and hence critical deceleration, happens according to Eq. (10.2.14) and because of $\gamma = \gamma_e$ when

$$\frac{da}{d\lambda} \propto \frac{d}{d\lambda}\left(\lambda e^{-\lambda}\right) = (1-\lambda)e^{-\lambda} = 0$$

and therefore at

$$\lambda_{crit} = 1 \tag{10.3.11}$$

Remark *In hindsight we recognize that the choice of the factor 2 in the definition* Eq. (10.2.12) *was motivated to have* λ_{crit} *unity.*

From Eq. (10.2.12) follows that $\lambda_{crit} = 1$ corresponds to the critical deceleration altitude

$$h_{crit} = H\ln\frac{2\kappa_D}{\sin\gamma_e} \tag{10.3.12}$$

From Eq. (10.2.14) we finally obtain for the critical deceleration

$$a_{crit} = \left(g_0 - \frac{v_e^2}{2eH}\right)\sin\gamma_e \approx -\frac{v_e^2\sin\gamma_e}{2eH} \tag{10.3.13}$$

The last three equations mark the ball-park of the results for reentries with lift and gravitational perturbations to which we turn after the next section.

10.3.3 Heat Flux

As stated in our thermal problem setting in Sect. 10.1.1, it is our goal to determine the peak heat flux in the course of reentry. Quite generally, the heat flux on a S/C at the stagnation point is according to Eq. (10.1.3)

$$\dot{q}_{S/C} = \frac{St}{2}\sqrt{\rho\rho_q\frac{R_0}{R_n}}\cdot v^3$$

To find the maximum $\dot{q}_{S/C}(v)$ we need to have the dependency of ρ from the speed. From Eq. (10.2.12)

$$\lambda = \frac{BH}{\sin\gamma_e}\rho$$

where $B = C_D A_\perp / m$ is the ballistic coefficient (see Eq. (6.2.19)). We know from the numerical calculations that the maximum deceleration occurs where the body first deviates from the straight trajectory. Because we expect the maximum heating around maximum deceleration we apply for a ballistic reentry the basic solution Eq. (10.3.7), $v = v_e e^{-\lambda/2}$. The atmospheric density as a function of v then is determined to be

$$\rho = 2\frac{\sin\gamma_e}{BH}\ln\frac{v_e}{v}$$

Hence

$$\dot{q}_{S/C} = \frac{St}{2}\sqrt{2\rho_q\frac{R_0}{R_n}\frac{\sin\gamma_e}{BH}}\cdot\sqrt{\ln\frac{v_e}{v}}\cdot v^3$$

As $\dot{q}$ is monotonous in v, this results in the condition equation for a maximum $\dot{q}$

$$\frac{1}{\dot{q}}\frac{d\dot{q}}{dt} \propto \frac{1}{\dot{q}}\frac{d\dot{q}}{dv} = \frac{1}{v\ln(v/v_e)}\left(\frac{1}{2} - 3\ln\frac{v}{v_e}\right) = 0$$

From this follows that

$$v_{\max\dot{q}} = \frac{v_e}{e^{1/6}} = 6.3\ \mathrm{km\ s^{-1}}\cdot\sqrt{\varepsilon_e} \approx 6.3\ \mathrm{km\ s^{-1}} \tag{10.3.14}$$

Remark *If we would have assumed the Detra and Hidalgo heat flux model with* $\dot{q}_{S/C} \propto \sqrt{\rho}\, v^{3.15}$ *we would have derived for the critical velocity* $v_{\max\dot{q}} = v_e e^{-1/6.3}$, *which deviates by only 1% from the above result.*

So the S/C experiences its maximum heating even far before its critical deceleration at $v_{crit} = 4.5\,\mathrm{km\,s^{-1}}$ (see Eq. (10.4.17)). The altitude where the maximum heating is reached is derived from $v = v_e e^{-\lambda/2}$ as $\lambda_{\max\dot{q}} = 1/3$ and because of Eq. (10.2.12)

$$h_{\max\dot{q}} = H\ln\frac{6\kappa_D}{\sin\gamma_e} = h_{crit} + 1.10H \approx h_{crit} + 8.8\ \mathrm{km} \tag{10.3.15}$$

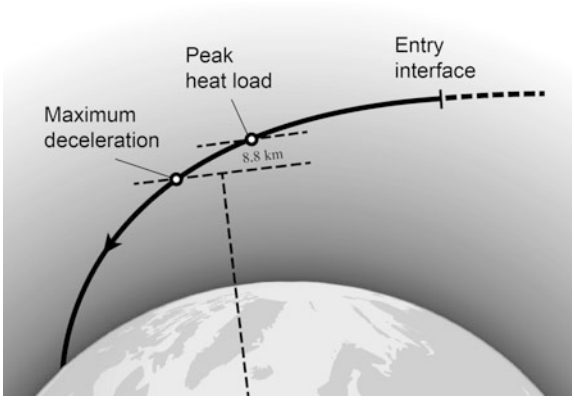

Fig. 10.9 Occurrence of peak heat load and maximum deceleration for a ballistic reentry

with $H = 8.0$ km. This relation is qualitatively depicted in Fig. 10.9. For a typical ballistic entry angle $\gamma_e \approx 3°$ (see Soyuz reentry in Sect. 10.1.3) we have $h_{\max \dot{q}} \approx 60$ km. For $\gamma_e = 3° - 10°$ maximal heating therefore occurs at an altitude of about 55 km and for high entry angles, $\gamma_e \approx 45°$, at 41 km.

Finally, the peak heat flux at the stagnation point of the S/C is found to be

$$\dot{q}_{S/C\,\max} = \frac{St}{2} \cdot v_e^3 \sqrt{\frac{\rho_q \sin\gamma_e}{3e \cdot BH} \frac{R_0}{R_n}} = \dot{q}_e \left(\frac{v_e}{v_\triangleright}\right)^3 \sqrt{\frac{\sin\gamma_e}{3e\rho_e BH} \frac{R_0}{R_n}} \tag{10.3.16}$$

with $\dot{q}_e = \frac{St}{2}\sqrt{\rho_q \rho_e} v_\triangleright^3 = 1.15$ W cm^{-2} the standard heat flux at entry interface, where $St = 0.001, v_\triangleright = 7.905$ km s^{-1}, $R_0 = 1$ m, $\rho_q = 0.121$ kg m^{-3} and $\rho_e = 1.80 \times 10^{-8}$ kg m^{-3} the mean atmospheric density at entry interface according to MSIS-E-90. Observe that the heat flux is reduced by a larger radius of curvature, R_n, and by a larger ballistic coefficient $B = C_D A_\perp / m$. Note that the expression $\rho_e BR$ and hence the entire square root is dimensionless and that $\rho_e BH$ relates to Bstar, B^*, of NORAD's TLE (see Remark in Sect. 12.7.3) as

$$\rho_e BH = 2B^* \frac{\rho_e}{\rho_{120}} \frac{H}{R} = 1.46 B^* \frac{H}{R}$$

where the latter holds only if the actual atmospheric density at entry interface is the standard value $\rho_{120} \equiv \rho_0 = 2.461 \times 10^{-8}$ kg m^{-3} as assumed in the Simplified General Perturbation Model SGP of NORAD.

With this and Eq. (10.1.1) the peak temperature at this point is calculated to be

$$T_{\max}^4 = \frac{T_e^4}{\varepsilon} \cdot \left(\frac{v_e}{v_\triangleright}\right)^3 \sqrt{\frac{\sin\gamma_e}{3e\rho_e BH} \frac{R_0}{R_n}} \tag{10.3.17}$$

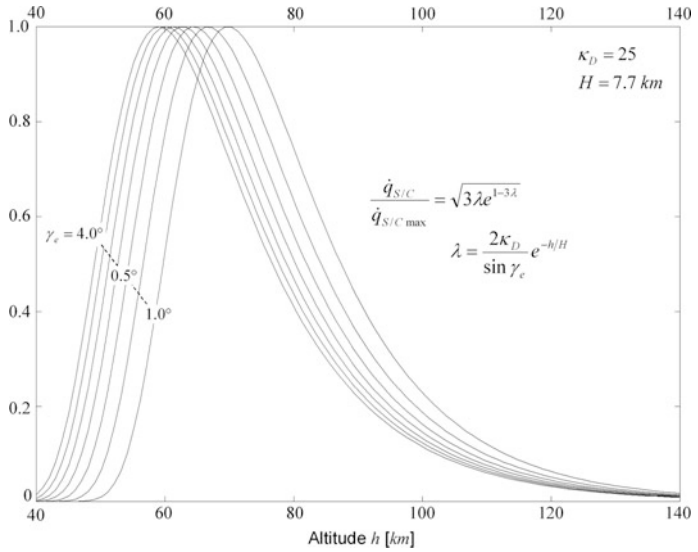

Fig. 10.10 Normalized ballistic reentry heat flux at the stagnation point of a spacecraft as a function of altitude h and entry angle γ_e in steps of 0.5°

with

$$T_e = \left(\frac{\dot{q}_e}{\sigma}\right)^{1/4} = 671\ \mathrm{K}$$

the standard stagnation point temperature at entry interface and $\varepsilon \approx 0.85$ the approximate emissivity of the heat shield. With Eq. (10.3.16) we can rewrite Eq. (10.1.3) to a normalized heat flux on the S/C as

$$\frac{\dot{q}_{S/C}}{\dot{q}_{S/C\,\max}} = \sqrt{3\lambda e^{1-3\lambda}} \tag{10.3.18}$$

This function is plotted in Fig. 10.10 for various entry angles.

As will be shown at the end of Sect. 10.4.2 all considerations in this section for the calculation of the heat flux for a ballistic reentry are also valid for the general reentry case. Therefore, all findings in this Sect. 10.3.3 are elementary results (except for lifting reentry, see Sect. 10.6.3).

10.4 Reentry with Lift

10.4.1 Lift-Only Case

We now make a step forward to solve the basic differential Eq. (10.2.13) for reentry by allowing for a lift of the reentry vehicle, but still neglecting gravitational and centrifugal forces via $H/R = 0$ (see explications following Eq. (10.2.13)). The differential equations then read

$$\frac{d(\ln \varepsilon)}{d\lambda} = -\frac{\sin \gamma_e}{\sin \gamma}$$
$$\frac{d(\cos \gamma)}{d\lambda} = \frac{\sin \gamma_e}{2} \frac{L}{D}$$

We recall from Eq. (10.2.13) that we assume $L/D \approx const$. In fact, L and D depend somewhat differently on speed and angle of attack, so that L/D slightly depends on speed and AOA. Within our approximations (see Sect. 10.3) $L/D = const$, however, is a good assumption, which we will adopt from now. This permits to solve the second equation directly by separating the variables

$$\cos \gamma = (1 + b\lambda) \cos \gamma_e \tag{10.4.1}$$

where the constant

$$b := \frac{\tan \gamma_e}{2} \frac{L}{D} \tag{10.4.2}$$

describes the lift power (buoyancy) and $1 + b(\lambda - \lambda_e) \approx 1 + b\lambda$. What does this quite important equation tell us? The vehicle entries the atmosphere at the entry interface $\lambda = \lambda_e$ with $\gamma = \gamma_e$. Since it descends, λ increases. According to Eq. (10.4.1) a positive lift, $b > 0$, decreases the flight path angle steadily until $\cos \gamma = 1$, when a horizontal flight with $\gamma = 0$, is attained. Of course, lift continues to act on the vehicle, which leads now to an increase in altitude and hence a decreasing λ, which via Eq. (10.4.1) in turn implies $\cos \gamma < 1$ anew, but this time with a negative flight path angle $\gamma < 0°$. In total, the positive lift results in a steadily upward curved trajectory (cf. the numerical calculations in Sect. 10.2.1). If lift is negative, that is if the reentry body turns upside down, then the trajectory steadily turns down. From Eq. (10.4.1) we find after some minor trigonometric conversions

$$\sin \gamma \approx \sin \gamma_e \sqrt{1 - 2c\lambda} \tag{10.4.3}$$

with constant

$$c := b\cot^2\gamma_e = \frac{\cot\gamma_e}{2}\frac{L}{D}$$

where we have neglected the term of order $b^2\lambda^2$ in the root, which is equivalent to $\lambda L/D \ll 4\cot\gamma_e$, and which typically holds for altitudes $h > H\ln(100L/D)$. We insert this expression into the first differential equation to find

$$d(\ln\varepsilon) = -\frac{\sin\gamma_e}{\sin\gamma}d\lambda = -\frac{d\lambda}{\sqrt{1-2c\lambda}}$$

We can solve this equation analytically to arrive at

$$\ln\frac{v}{v_e} = \frac{1}{2c}\left(\sqrt{1-2c\lambda}-1\right) \quad @ \quad \lambda\frac{L}{D} \ll 4\cot\gamma_e \tag{10.4.4}$$

This solution holds for any L/D values, even for a high-lift reentry, as long as $\lambda L/D \ll 4\cot\gamma_e$. There even exists a fully analytical solution without the approximation $\lambda L/D \ll 4\cot\gamma_e$. But because this is much more complex and because it does not help to understand we pursue it in an exercise (Problem 10.6). As expected, Eq. (10.4.4) passes over into Eq. (10.3.6) for $L/D \propto c \to 0$.

10.4.2 General Results

After these introductory considerations we now make the final step forward in solving the reentry equations of motion by allowing for the perturbative terms of gravitation and centrifugal forces

$$\frac{d(\ln\varepsilon)}{d\lambda} = -\frac{\sin\gamma_e}{\sin\gamma} + \frac{2H}{\varepsilon\lambda R}$$
$$\frac{d(\cos\gamma)}{d\lambda} = \frac{\sin\gamma_e}{2}\frac{L}{D} - \left(\frac{1}{\varepsilon}-1\right)\frac{H\cos\gamma}{\lambda R}$$

Because $H/R \approx 0.001$ we assume the H/R-terms to be gravitational perturbations of first order with respect to the terms considered so far. We will take these perturbations fully into account. However, because they are small, it will suffice to apply for $\cos\gamma$ and ε the undisturbed terms of Sect. 10.3.2 in these perturbative terms, i.e., we will not consider perturbations of perturbations. With this so-called second-order perturbation analysis we are looking for solutions. These solutions will not be globally exact (we already know that there are no globally exact solutions), but they will be applicable for a quite extended region of λ.

Flight Path Angle

For $\cos\gamma$ and ε we insert the unperturbed expressions from Eqs. (10.3.5) and (10.3.6). The γ equation then reads

$$d(\cos\gamma) = \left[\frac{\sin\gamma_e}{2}\frac{L}{D} - \left(\frac{e^\lambda}{\varepsilon_e} - 1\right)\frac{H}{\lambda R}\cos\gamma_e\right]d\lambda$$

from which by direct integration follows

$$\cos\gamma = \left[1 + b\lambda - \frac{H}{\varepsilon_e R}\int_{\lambda_e}^{\lambda}\frac{e^x - \varepsilon_e}{x}dx\right]\cos\gamma_e$$

where again $1 + b(\lambda - \lambda_e) \approx 1 + b\lambda$. The integral that comprises the perturbation can be solved analytically

$$\int_{\lambda_e}^{\lambda}\left(\frac{e^x}{x} - \frac{\varepsilon_e}{x}\right)dx = Ei(\lambda) - Ei(\lambda_e) - \varepsilon_e \ln\frac{\lambda}{\lambda_e}$$

We find from any special formulary that the exponential integral $Ei(x)$ can be expressed as

$$Ei(\lambda) - Ei(\lambda_e) = f^\lambda - f^{\lambda_e} + \ln\frac{\lambda}{\lambda_e} \approx f^\lambda + \ln\frac{\lambda}{\lambda_e} \tag{10.4.5}$$

where we have defined the exponential-like function

$$f^x := \int_0^x \frac{e^y - 1}{y}dy = \sum_{n=1}^{\infty}\frac{x^n}{nn!} \tag{10.4.6}$$

Due to the global convergence of this power series this function can easily be calculated numerically and is depicted in Fig. 10.11. We therefore find with Eq. (10.2.12)

$$\chi(\lambda, \varepsilon_e) := \int_{\lambda_e}^{\lambda}\frac{e^x - \varepsilon_e}{x}dx = f^\lambda - (\varepsilon_e - 1)\ln\frac{\lambda}{\lambda_e} \approx f^\lambda - (\varepsilon_e - 1)\frac{h_e - h}{H} \tag{10.4.7}$$

where we have defined the chi function $\chi(x, \varepsilon)$ that is related to the f function by $\chi(x, 1) = f^x$.

The solution for the flight path angle therefore is

$$\cos\gamma = [1 + b\lambda - p\chi(\lambda, \varepsilon_e)]\cos\gamma_e \quad \textbf{FPA equation} \tag{10.4.8}$$

where

$$p := \frac{H}{\varepsilon_e R} \approx 0.001 \ll 1$$

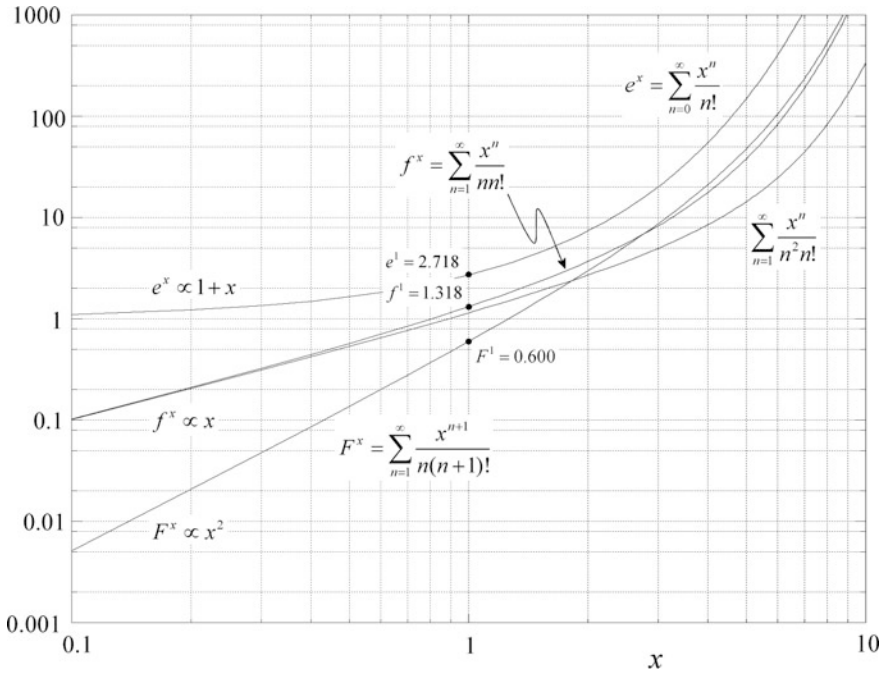

Fig. 10.11 Representation of the functions f^x, F^x as defined in the text and e^x

signifies the strength of the gravitational perturbation (see gravity term in Eq. (10.2.13a)). The FPA Eq. (10.4.8) is the full-fledged version of Eq. (10.4.1) for a general reentry and hence is of high significance for understanding reentry. It indirectly describes the course of the reentry trajectory with altitude for any entry condition. Because of these properties we will make use of it for equilibrium reentries.

Let us have a closer look at the reentry behavior with the FPA equation. For $\varepsilon_e = 1$ at high altitudes $\chi(\lambda, 1) \approx \lambda \ll 1$. Therefore, $\cos\gamma \approx \cos\gamma_e$: the entry vehicle descends on a straight line. With decreasing altitude λ and hence $\chi(\lambda, 1)$ increases exponentially. Since $b = 0.01 - 0.1$ while $p \approx 0.001$, the lift term $b\lambda$ incipiently is more significant than $p\chi$. It increases $\cos\gamma$, so γ decreases: The vehicle will slowly deviate upward from the straight line. At lower altitudes, $\lambda > 1, \chi$ increases exponentially with λ (therefore double-exponentially with decreasing h) so the gravity term quickly becomes significant. The specific value of $b = L \cdot \tan\gamma_e/(2D)$ depends on the entry angle and the lift. If it is quite substantial, the right-hand side of Eq. (10.4.8) at some point becomes unity where the vehicle flies horizontally. But because the lift continuously lifts the vehicle it begins to ascent ($\gamma < 0$), implying a decreasing $\cos\gamma$, because also λ decreases. So, if b if sufficiently big, the vehicle may reverse the flight path angle and ascent before gravity overcomes this excursion. If b is too small, then there is just an indication of an upturn, but gravity will beat it soon. This is exactly what we see in the numerical calculations Figs. 10.5, 10.6 and 10.7.

Critical Deceleration
The critical deceleration a_{crit}, that is the maximum deceleration during reentry, can be derived from Eq. (10.2.14). We rearrange this equation to

$$a = -g_0 \frac{R \sin\gamma_e}{2H} \left(\varepsilon\lambda - \frac{2H}{R} \frac{\sin\gamma}{\sin\gamma_e} \right)$$

We now apply second-order perturbation analysis: Because H/R is a perturbation $\sin\gamma \approx \sin\gamma_e$, and hence

$$a = -g_0 \sin\gamma_e \left(\frac{\varepsilon\lambda R}{2H} - 1 \right) \tag{10.4.9}$$

This expression is no longer exact, but because even for extremely flat entry angles $\varepsilon_{crit}\lambda_{crit} \geq 0.1$ and because $2H/R = 0.0021$, this still is a very good approximation for all practical purposes. From the maximum condition $da/d\lambda = 0$, we derive from Eq. (10.4.9) in a few steps the critical λ to be

$$\lambda_{crit} = \left[1 + \frac{2H}{\varepsilon_{crit} R} \right] \frac{\sin\gamma_{crit}}{\sin\gamma_e} \tag{10.4.10}$$

We now could insert this into Eq. (10.4.9) to find the wanted a_{crit}. This, however, would in principle be not permissible because ε_{crit}, γ_{crit} in Eq. (10.4.10) themselves depend on λ_{crit}. But for the upcoming special cases this will be not a problem and Eq. (10.4.10) will therefore be of great value.

Heat Flux
What is the peak heating in the case of a reentry with lift? From Eq. (10.4.10) we see that the critical deceleration takes place at $\lambda_{crit} \approx 1$. Since we saw that the critical heating happens before that point, all the results of Sect. 10.3.3 for the peak heating for a ballistic reentry holds also for this general case.

10.4.3 Near-Ballistic Reentry

Up to this point we have solved the γ equation of motion including gravitational forces in second-order perturbation analysis. Now that we move on to solve also the ε equation this is no longer possible. If we still want to take gravitation into account, we can do so only by applying first-order perturbation analysis. So the following solutions will apply only for more restricted altitudes.

Entry Velocity
The problem is that we can no longer exactly integrate the expression $1/\sin\gamma = 1/\sqrt{1-\cos^2\gamma}$ with $\cos\gamma = [1 + b\lambda - p\chi(\lambda, \varepsilon_e)]\cos\gamma_e$. We can do so only with

linear approximations by assuming

$$c^2\lambda^2 \ll 1 \quad \text{and} \quad q^2\chi^2(\lambda, \varepsilon_e) \ll 1$$

with constants

$$c := b\cot^2\gamma_e = \frac{\cot\gamma_e}{2}\frac{L}{D}$$
$$q := p\cot^2\gamma_e = \frac{H}{\varepsilon_e R}\cot^2\gamma_e$$

which is equivalent to assuming a relatively steep reentry with low lift, i.e., a near-ballistic case. If these approximations hold we obtain

$$\sin\gamma \approx \sin\gamma_e\sqrt{1 - 2c\lambda + 2q\chi} \tag{10.4.11}$$

from which follows

$$\frac{\sin\gamma_e}{\sin\gamma} \approx \frac{1}{\sqrt{1 - 2c\lambda + 2q\chi}} \approx 1 + c\lambda - q\chi$$

We insert this result into the ε equation and separate the variables

$$d(\ln\varepsilon) = \left[-(1 + c\lambda - q\chi) + \frac{2H}{\varepsilon\lambda R}\right]d\lambda$$

Because the second term on the right-hand side is the perturbation we can adopt for ε the unperturbed expression from Eq. (10.3.6). With Eq. (10.4.11) and the approximations $c^2\lambda^2 \ll 1$ and $q^2\chi^2(\lambda, \varepsilon_e) \ll 1$ we then derive

$$\ln\frac{\varepsilon}{\varepsilon_e} = -\int_{\lambda_e}^{\lambda}(1 + c\lambda - q\chi)d\lambda + 2p\int_{\lambda_e}^{\lambda}\frac{e^x}{x}dx$$
$$\approx -\lambda - \frac{1}{2}c\lambda^2 + q\int_0^{\lambda-\lambda_e}\chi(x, \varepsilon_e)dx + 2p[Ei(\lambda) - Ei(\lambda_e)]$$

So we finally find with Eq. (10.4.5)

$$\ln\frac{v}{v_e} \approx -\frac{\lambda}{2} - \frac{1}{4}c\lambda^2 + \frac{q}{2}\mathrm{X}(\lambda, \varepsilon_e) + p\chi(\lambda, 0) \tag{10.4.12}$$

with

$$\mathrm{X}(\lambda, \varepsilon_e) := \int_0^{\lambda} \chi(x, \varepsilon_e) \cdot dx = F^{\lambda} - (\varepsilon_e - 1)\lambda\left(\ln\frac{\lambda}{\lambda_e} - 1\right)$$

where we have introduced the X function and F function

$$F^x := \int_0^x f^y dy = \sum_{n=1}^{\infty} \frac{x^{n+1}}{n(n+1)!}$$

which like f^x can easily be calculated numerically by the power series expansion. It is also depicted in Fig. 10.11.

Entry Trajectory

Within the first-order perturbation analysis, that is for $c^2\lambda^2 \ll 1$ and $q^2\chi^2(\lambda, \varepsilon_e) \ll 1$, it can be shown easily (exercise, Problem 10.4) that the course of the trajectory with altitude can be described analytically by

$$x \approx \cot\gamma_e \left\{(h_e - h) + \frac{H}{\sin^2\gamma_e}[b\lambda - p \cdot \Theta(\lambda, \varepsilon_e)]\right\} \tag{10.4.13}$$

with

$$\Theta(\lambda, \varepsilon_e) := \int_0^{\lambda-\lambda_e} \frac{\chi(x, \varepsilon_e)}{x} dx = \sum_{n=1}^{\infty} \frac{\lambda^n}{n^2 n!} - \frac{1}{2}(\varepsilon_e - 1)\ln^2\frac{\lambda}{\lambda_e}$$

Here x is the downrange distance relative to the entry point. This dependency is illustrated in Fig. 10.12 for an entry with $\gamma_e = 45°$. We recognize the straight entry line $x = \cot\gamma_e(h_e - h)$. The actual entry trajectory deviates from this for a positive lift by an upturn and for negative lift by a downturn. The trajectory representation ends where $c^2\lambda^2 \ll 1$ is no longer valid. The numerical solutions of the full equations of motion for this case show that for $L/D = 0.3$ the vehicle in the further course of the trajectory flies horizontally at 21 km altitude for a moment to finally descend. For $L/D = 0.4$, there is a reflection point at 23.5 km altitude, a maximum at 24.6 km altitude, and thereafter a final descend. For $L/D = 0.5$ the reflection point is at 25 km and the maximum at 30 km altitude.

Critical Deceleration

To determine λ_{crit} we employ the approximate solutions of $\varepsilon(\lambda)$ and $\sin\gamma(\lambda)$ for the unperturbed reentry from Eqs. (10.3.6) and (10.4.3) and obtain for this first-order perturbation analysis

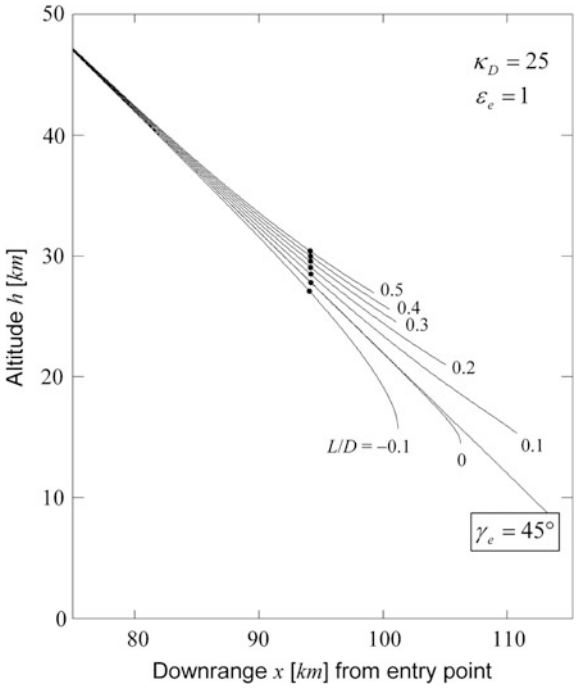

Fig. 10.12 Reentry trajectories for $\gamma_e = 45°$ as given by Eq. (10.4.13) for different L/D ratios. On the x-axis is the downrange distance from entry point. The full dots denote the critical altitudes

$$\lambda_{crit} = (1 + 2ep)\sqrt{1 - 2c + 2q\chi(1, \varepsilon_e)}$$

with

$$\chi(1, \varepsilon_e) = 1.318 - (\varepsilon_e - 1) \ln \frac{1}{\lambda_e}$$

and

$$\ln \frac{1}{\lambda_e} = 18.2 - \ln \frac{2\kappa_D}{\sin \gamma_e}$$

Because $2ep = 2eH/\varepsilon_e R < 0.0065$, this term is negligible and therefore we find with the definition of c from Eq. (10.4.3)

$$\lambda_{crit} = \sqrt{1 - 2c + 2q\chi(1, \varepsilon_e)} = \sqrt{1 - \cot \gamma_e \frac{L}{D} + 2 \cot^2 \gamma_e \frac{H}{\varepsilon_e R} \chi(1, \varepsilon_e)} \quad (10.4.14)$$

Note *Because we have assumed* $c, p \ll 1$, *essentially* $\lambda_{crit} \approx 1$. *Lift and gravity cause only minor variations from this value.*

The critical altitude at which the critical deceleration happens is determined from Eq. (10.2.12) as

$$h_{crit} = H \ln \frac{2\kappa_D}{\lambda_{crit} \sin \gamma_e} \quad \textbf{critical deceleration altitude} \tag{10.4.15}$$

Note *Because* $\lambda_{crit} \approx 1$ *also holds for very flat lifting reentries* (see Sect. 10.6; Eq. (10.6.7)), Eq. (10.4.15) *applies quite generally.*

Together with Eq. (10.4.14) this equation describes how the critical altitude changes as a function of lift and entry angle. It increases with increasing lift (see Fig. 10.12) and with decreasing entry angle. For $L \approx 0$ and $\gamma_e = 3^\circ - 10^\circ$ critical altitudes are about 43–52 km. We recall that for the above derivation of λ_{crit} we used approximate differential equations that do not reproduce the intricate trajectory of flat reentries as depictured in Figs. 10.6 and 10.7. The critical deceleration therefore always refers to the first deceleration phase at the commencement of reentry, which for very flat reentries might be lower than decelerations on later reentries after skipping (see Figs. 10.7 and 10.13b).

For the critical deceleration we apply Eq. (10.4.9) to the critical point. Inserting Eq. (10.4.14) yields for $c^2\lambda^2 \ll 1$ and $q^2\chi^2(\lambda, \varepsilon_e) \ll 1$

$$a_{crit} = -\frac{v_e^2 \sin \gamma_e}{2eH}\left[1 - \frac{1}{4}\cot\gamma_e \frac{L}{D} + \frac{H}{\varepsilon_e R}(\xi - 2e)\right] \quad \textbf{critical deceleration} \tag{10.4.16}$$

with constant

$$\xi(\varepsilon_e) := 2.636 + (\varepsilon_e - 0.400) \cdot \cot^2 \gamma_e - \left[\cot^2 \gamma_e(\varepsilon_e - 1) - 2\right] \ln \frac{1}{\lambda_e}$$

The velocity at which the deceleration becomes maximal is determined from Eq. (10.4.12) to be

$$v_{crit} = \frac{v_e}{\sqrt{e}}\left[1 - \frac{\cot\gamma_e}{8}\frac{L}{D} + \frac{H}{2\varepsilon_e R}\xi(\varepsilon_e)\right] \approx \frac{v_e}{\sqrt{e}} = 4.5 \text{ km/s} \cdot \sqrt{\varepsilon_e} \tag{10.4.17}$$

For the latter we have chosen $v_e = 7.44$ km/s, which is more realistic, because due to the Earth's rotation the entry velocity with respect to the atmosphere is effectively reduced.

Reentry from LEO

For a reentry from LEO we have $\varepsilon_e = 1$ and therefore

$$\xi - 2e = 0.600 \cdot \cot^2 \gamma_e + 33.6 - 2 \ln \frac{2\kappa_D}{\sin \gamma_e} \approx 0.600 \cdot \cot^2 \gamma_e + 21.0$$

and therefore

$$a_{crit} = -\frac{v_0^2 \sin \gamma_e}{2eH} \left(1.025 - \frac{1}{4} \cot \gamma_e \frac{L}{D} + 6.30 \times 10^{-4} \cot^2 \gamma_e \right) \quad @ \quad \varepsilon_e = 1$$

Because $v_0^2/(2eH) = Rg_0/(2eH) = 154 \cdot g_0$, we finally obtain

$$\boxed{a_{crit} = -154 \cdot g_0 \sin \gamma_e \left(1.025 - \tfrac{1}{4} \cot \gamma_e \tfrac{L}{D} + 6.30 \cdot 10^{-4} \cot^2 \gamma_e\right)} \quad @ \quad \varepsilon_e = 1 \tag{10.4.18}$$

For decreasing entry angles the critical deceleration deviates more and more from the simple relationship $a_{crit} = -154 \cdot g_0 \varepsilon_e \sin \gamma_e \cdot 1.025 = -158 \cdot g_0 \varepsilon_e \sin \gamma_e$ (see Fig. 10.13a) to larger values. This is counteracted by a positive lift. In Fig. 10.13a, the critical deceleration for $\varepsilon_e = 1$ is plotted according to Eq. (10.4.18) for different L/D.

For $\gamma_e \leq 1.5°$ our approximations definitely no longer apply, because $\cot \gamma_e$ diverges. On the other hand $\sin \gamma_e \to 0$. One could presume that overall a_{crit} would converge for $\gamma_e \to 0$. Numerical calculations that continue the analytical solutions for $\gamma_e \leq 1.5°$ (see Fig. 10.13) corroborate this supposition. With a semi-analytical ansatz V. A. Yaroshevsky in 1964 could even show that for $L = 0$ and with $H = 7.6$ km (see Eq. (10.3.3)), the critical deceleration for $\gamma_e \to 0$ converges to $a_{crit} = 0.277 \cdot g_0 \sqrt{R/H} = 8.0\, g_0$. This is in excellent agreement with our numerical calculations. This limiting case, however, is of no practical interest, since for $\gamma_e \to 0$ the downrange distance becomes infinite. It is just the other way round that, to determine precisely the landing site of a capsule, the downrange distance should be as small and hence the entry angle as large as possible.

These contradictory requirements can only be resolved by a capsule with lift. We therefore provide in Fig. 10.13b a fully numerical calculation for $-0.5 \leq L/D \leq 0.6$ based on the MSIS-E-90 atmospheric model.

Example

For manned missions the reentry trajectory is chosen such that the critical deceleration never exceeds the maximum tolerable value of 10 g. From Fig. 10.13b it follows that for ballistic entries, $L = 0$, from LEO $\gamma_e < 3.1°$. Of course no astronaut wants to pull 10 g. Therefore, reentry with the Soyuz capsule is limited to 4.5 g. According to Fig. 10.13a this corresponds to an entry angle of 3.9° at a lift of $L/D = 0.3$, which is typical for capsules with a heat shield.

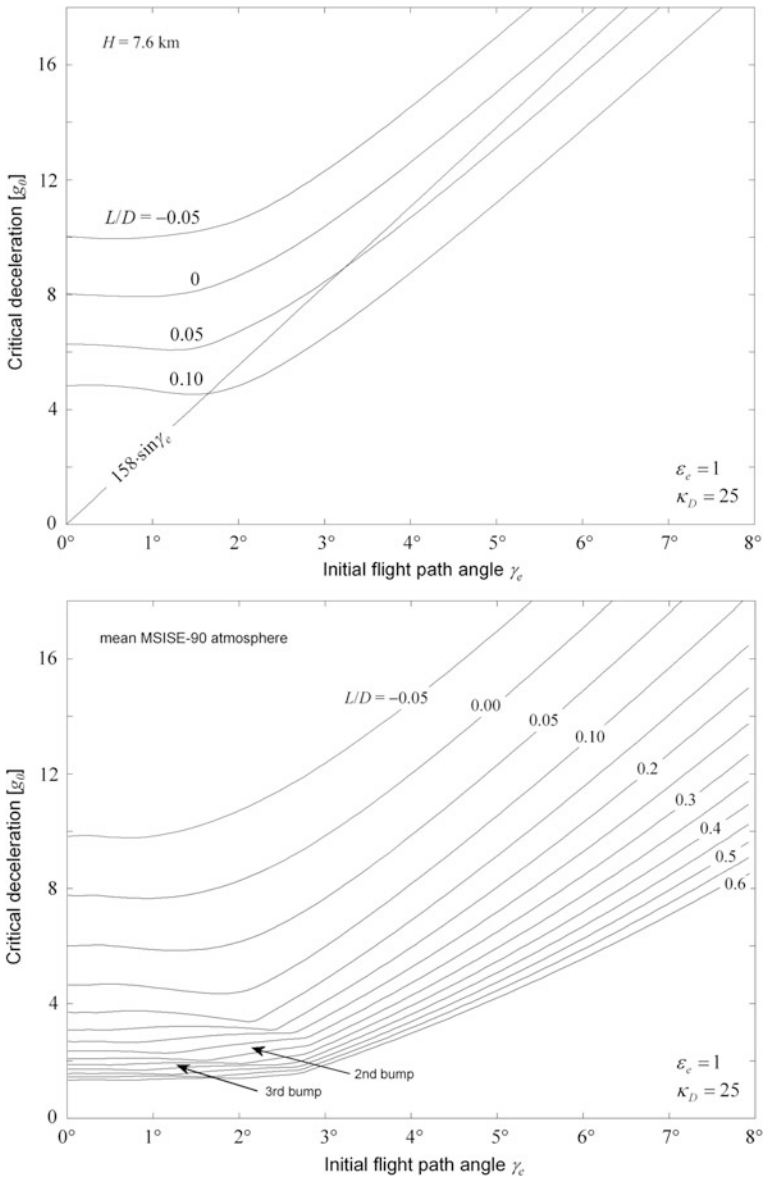

Fig. 10.13 The critical deceleration as a function of the initial flight path angle (entry angle) and lift. **a** Approximate calculations as from Eq. (10.4.18), for small $\cot\gamma_e L/D$, i.e., for $L/D \leq 0.1$ and $\gamma_e > 1.5°$. Results for $\gamma_e \leq 1.5°$ are numerical solutions. **b** Fully numerical calculations with a mean MSIS-E-90 atmospheric model (cf. Sect. 6.1.3) for $L/D \leq 0.6$. The critical deceleration occurs at the first deceleration maximum, except for areas indicated by "2nd bump" and "3rd bump" where it happens at the second maximum (cf. Fig. 10.7) and third maximum, respectively. Differences between (**a**) and (**b**) result from the different atmospheric models used

10.5 Reflection and Skip Reentry

10.5.1 Reflection

From the discussion of the FPA Eq. (10.4.8) we saw that it nicely reproduces the upturn of the reentry trajectory for positive lift. In fact, we can take the FPA equation to determine the point—the reflection point—where the vehicle turns back to increasing altitudes. From the reflection condition $\cos\gamma = 1$ we derive from (10.4.8) for the reflection altitude λ_r

$$1 + \frac{\tan\gamma_e}{2}\frac{L}{D}\lambda_r - \frac{H}{\varepsilon_e R}\chi(\lambda_r, \varepsilon_e) - \frac{1}{\cos\gamma_e} = 0 \tag{10.5.1}$$

Reflections typically take place at $h_r > 20\,\text{km} \rightarrow \lambda_r < 3$, where according to Fig. 10.11 $\chi(3, \varepsilon_e \approx 1) = f^3 \approx 10$. Therefore, $H\chi/\varepsilon_e R \ll 1$, which implies that Eq. (10.5.1) can be reduced to

$$1 + \frac{\tan\gamma_e}{2}\frac{L}{D}\lambda_r - \frac{1}{\cos\gamma_e} = 0 \tag{10.5.2}$$

From this and with Eq. (10.2.12) it follows for the reflection altitude

$$h_r = H\ln\left(\frac{L}{D}\frac{\kappa_D}{1-\cos\gamma_e}\right) \quad \textbf{reflection altitude} \tag{10.5.3}$$

Figure 10.14 shows the reflection altitudes as a function of the entry angle for a given L/D and entry angle as calculated from Eq. (10.5.1). The results are almost identical to those from Eq. (10.5.3) except for $L/D < 0.2$ and $\gamma_e < 20°$, because then the gravity term is no longer negligible compared to the lift term.

> **Note** *The reflection altitude is independent from the entry velocity! One would have expected that it decreases with increasing entry speed because a higher entry momentum defies the ability to turn the vehicle up. But, on the other hand, the lifting force, which does the turn, increases quadratically with speed* (*cf. Eq.* (10.2.5))*, which just compensates the higher inertia of the vehicle.*

What are the entry parameters for which a reflection occurs? The condition derived from Eq. (10.5.1) reads

$$\frac{L}{D} \geq \left(\frac{1}{\cos\gamma_e} - 1\right)\frac{1}{\lambda_r} + \frac{H}{\varepsilon_e R}\frac{\chi(\lambda_r, \varepsilon_e)}{\lambda_r} \tag{10.5.4}$$

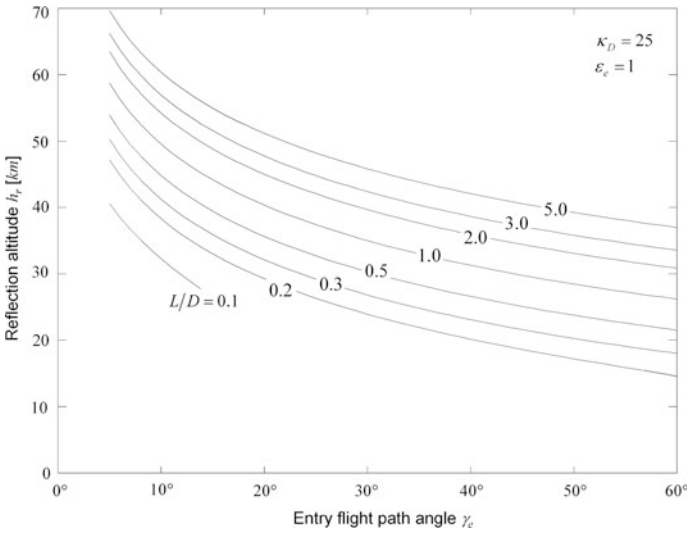

Fig. 10.14 Reflection altitudes as a function of the entry angle and lift for $\varepsilon_e = 1$ (as derived from Eq. (10.5.1))

This equation states that the vehicle reflects at given λ if L/D satisfies this equation. We are now seeking that minimal L/D for which reflection sets in at altitude $\lambda_{r,hor}$, that is, where it just flies horizontally for the first time. Minimizing the term on the right-hand side of Eq. (10.5.4) delivers the condition equation

$$\left(\frac{1}{\cos\gamma_e} - 1\right) + \frac{H}{\varepsilon_e R}\left[e^{\lambda_{r,hor}} - \varepsilon_e - \chi\left(\lambda_{r,hor}, \varepsilon_e\right)\right] = 0 \tag{10.5.5}$$

The root of this equation for a given entry angle, which can be determined numerically, delivers $\lambda_{r,hor}$ and hence $h_{r,hor}$. Inserting it into Eq. (10.5.4) one obtains the wanted minimal L/D for a given entry angle. This dependency is displayed in Fig. 10.15 for $\varepsilon_e = 1$ and $\varepsilon_e = 2$.

If reflection is not desirable at all, then $L/D < 0.1$ has to be ensured. This can be achieved either by a continuous rotation of the capsule (which was done with Mercury), which ensures $\langle L/D\rangle_t = 0$ on a time average, or by turning the capsule sideways or even upside down such that the lift vector points down implying $L/D < 0$.

In course of the trajectory after reflection the vehicle speed quickly diminishes so that gravitation, $p\chi \approx 1$, outweighs the lift and therefore the S/C descends. This second entry phase, induced by the relentless gravitation, is not reflected by the term χ, though, because we assumed in the perturbation term of the γ equation just $\varepsilon = \varepsilon_e \exp(-\lambda)$. What in fact happens is as follows. Because in the ε equation $d\varepsilon \propto -d\lambda/\sin\gamma$, the velocity always decreases, independently whether the S/C ascends $(d\lambda < 0, \sin\gamma < 0)$ or descends $(d\lambda > 0, \sin\gamma > 0)$ and therefore also its

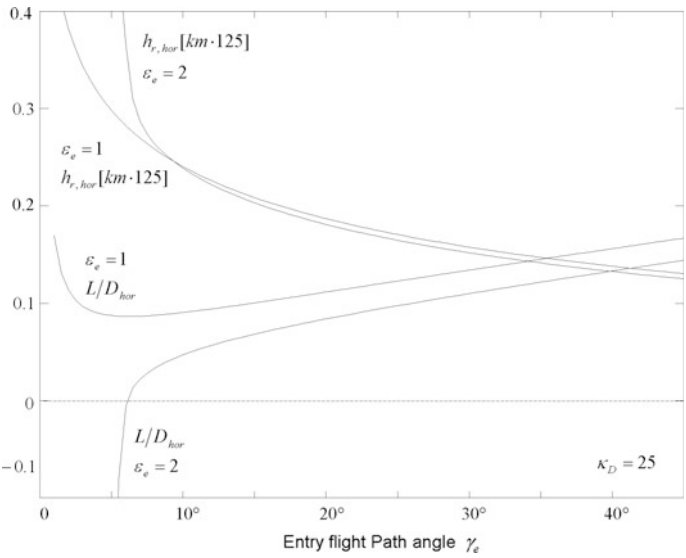

Fig. 10.15 Minimum values for *L/D* and corresponding altitudes at which reflection of a reentering vehicle sets in, for $\varepsilon_e = 1$ and $\varepsilon_e = 2$

energy $\varepsilon \propto v^2$ decreases steadily. Therefore, the term $-H\cos\gamma/\varepsilon\lambda R$ in the γ equation steadily increases, and at some time becomes of the order unity, independently from the flight path angle. It then dominates the lift and after the reflection at negative flight path angles $\gamma < 0$ forces the vehicle to turn down $d(\cos\gamma) \propto -d\lambda > 0$, and when it begins to descend again, $\gamma > 0$, to turn down even more rapidly $d(\cos\gamma) \propto -d\lambda < 0$. This behavior that we have derived from the equations of motion just reflects the fact that lift declines quadratically with decreasing speed so that gravity takes over and makes the vehicle sink in the long run. In order to verify this behavior in detail from the equations of motions, one has to solve the time-dependent form Eqs. (10.2.7) and (10.2.14) numerically. To apply for the analysis the reduced equations of motions Eq. (10.2.13) with λ as the independent variable, which has to progress per definition, would be useless, because after reflection λ actually decreases. So the λ-dependent γ Eq. (10.2.13b) cannot provide us a trajectory after reflection.

Moderate reflections are usually desirable for capsule reentries because they decrease speed without an increase of deceleration. We now will see how reflections can be driven into the extreme to utilize them for achieving moderate reentry decelerations for manned missions even at very high entry speeds as from interplanetary missions.

10.5.2 Skip Reentry

A skip reentry is the smart utilization of reflections to purposefully reduce the critical deceleration. It was used for the first time for the reentries of Apollo capsules after the return from the Moon. Here the entry velocity roughly corresponded to the second cosmic velocity of 11 km/s, and thus the entry energy was $\varepsilon_e = 2$. So the mission managers encountered the big problem to handle twice the amount of kinetic energy, as compared to the preceding Mercury and Gemini low Earth orbit missions and this seemed to be a special challenge for thermal protection and critical deceleration. The problem was solved by skip reentry (see Fig. 10.16). For reentry $\gamma_e \approx 6.5^\circ$ was chosen and the design of the capsule was laid out such that the center of mass of the capsule did not coincide with the center of pressure to obtain a $L/D \approx 0.3$. From Fig. 10.15 it can be seen that for $\varepsilon_e = 2$ and $\gamma_e \approx 6.5^\circ$ reflections occur for $L/D > 0$. $L/D = 0.3$ was therefore a sure choice. Such an intentional reflection with a subsequent ballistic coast is called a "skip". By means of skipping the initial speed can be reduced to such an extent that in a second dip reentry the deceleration forces are tolerable (see Figs. 10.6 and 10.7). The key purpose of skipping is a recurring stepwise speed reduction.

Exit Velocity

How big is the speed reduction by one skip? To determine it we examine the equations of motions (10.2.1) and (10.2.2). From Sect. 10.3.1 we know that at critical altitudes 30 km $\leq h \leq$ 70 km, when drag is about maximum, the gravitational term can be neglected.

> **Note** *In the γ equation the reduced gravitational term has for $1 \leq \varepsilon_e \leq 2$ a more sustainable effect because of the surplus centrifugal force of the approaching S/C. This centrifugal force effectively increases the lift resulting in higher reflection altitudes, as will be found from the following calculations. So we are on the safe side.*

Neglecting the gravitational terms we derive from Eqs. (10.2.1) and (10.2.2)

$$\dot{v} = -\frac{D}{m}$$
$$v\dot{\gamma} = -\frac{L}{m}$$

In order to determine the speed reduction we need the dependency $v(\gamma)$ of the symmetric trajectory around the reflection point to apply the condition $\gamma_{out} = -\gamma_{in}$ at the entry interface. So we need to get rid of the time dependency. We do this by dividing the above equations yielding

$$\frac{\dot{v}}{\dot{\gamma}} = \frac{dv}{d\gamma} = v\frac{D}{L}$$

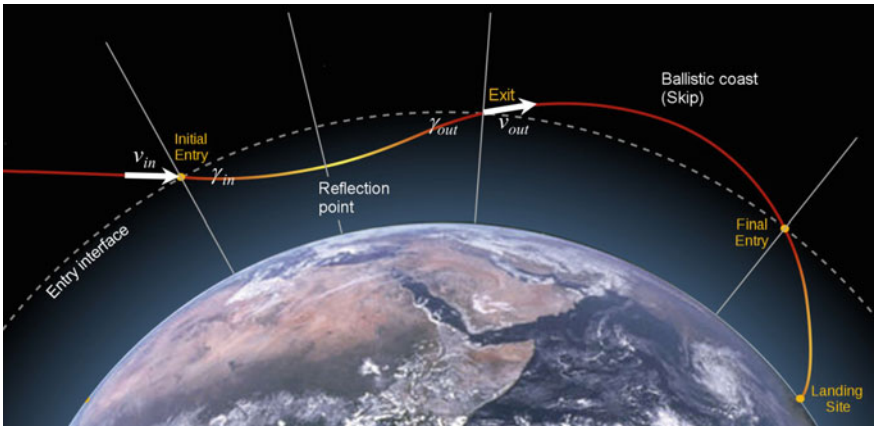

Fig. 10.16 Trajectory and trajectory parameters of a skip reentry. *Credit* Clem Tillier, Wikimedia Commons and U. Walter

From this follows with the initial conditions $v_{in} = v_e$, $\gamma_{in} = \gamma_e > 0$

$$\int_{v_{in}}^{v} \frac{dv}{v} = \frac{D}{L} \int_{\gamma_{in}}^{\gamma} d\gamma$$

and

$$v = v_{in} \exp\left[(\gamma - \gamma_{in})\frac{D}{L}\right]$$

As reflection implies an almost symmetrical flight path (see Fig. 10.16) about the reflection point, the condition

$$\gamma_{out} = -\gamma_{in}$$

has to be valid. So we get for the reduced exit velocity after reflection

$$v_{out} = v_{in} \exp\left(-2\gamma_{in}\frac{D}{L}\right) \tag{10.5.6}$$

Example

For the Apollo missions returning from the Moon the return velocity, and so the entry velocity of the capsule was $v_e = 11.0$ km s^{-1}. The selected entry angle was $\gamma_{in} = \gamma_e = 6.5°$ and the L/D ratio was $L/D = 0.3$. Therefore, and according to Eq. (10.5.6) the exit velocity after the reflection was $v_{out} = 0.470 \cdot v_e = 5.2$ km s^{-1}. With approximately this velocity the capsule was dipped again for a double dip (see below).

"Double Dip" Reentry with Apollo Flights

For reentries from outside LEO, there exists the so-called *entry corridor* for aerocapture, which for Apollo was only $5.0° < \gamma_e < 7.0°$ wide (see Figs. 10.17 and 10.3). For $\gamma_e > 7.0°$ the maximum admissible deceleration of 12 g would have exceeded during the skips. For $\gamma_e < 5.0°$ the splash down point would have been too imprecise due to an extended recoils from the atmosphere, or the risk of not or too weakly grazing the atmosphere for a skip would have been too large. This narrow corridor required a very precise approach from the Moon. In order to better determine the landing point for the Apollo and the Soviet Zond Moon flights, the so-called "double dip" reentry was used during the return process with a lift reversion: During the first reentry the lift vector was flown upward, as described above. After the reflection, however, the capsule was rotated so that the lift vector pointed downward (see Sect. 6.2.5), so that the negative lift kept the flight altitude roughly at the reflection altitude. With this maneuver it was possible to avoid bouncing back and the increasing inaccuracy of the landing point coming with this. In addition, the deceleration could be kept at lower altitudes to a more constant level, which altogether led to a safer landing.

Figure 10.18 depicts the historical reentry trajectory of Apollo 11. Judged against a comparable reentry trajectory from LEO (see Fig. 10.6) we recognize that the maximum after the first reflection is less developed. This is just the result of the negative lift. The reflection altitude of 185,000 ft = 56.5 km can easily be verified by applying Eq. (10.5.3) with the entry flight inclination angle of 6.5° and scale height $H = 8.0$ km at that altitude. This proves that the reflection altitude formula Eq. (10.5.3) is reliable and indeed is independent from the entry speed.

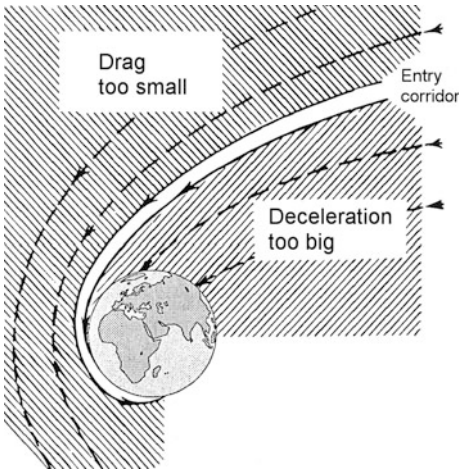

Fig. 10.17 Entry corridor for the return of the Apollo capsules from the Moon. *Credit* NASA

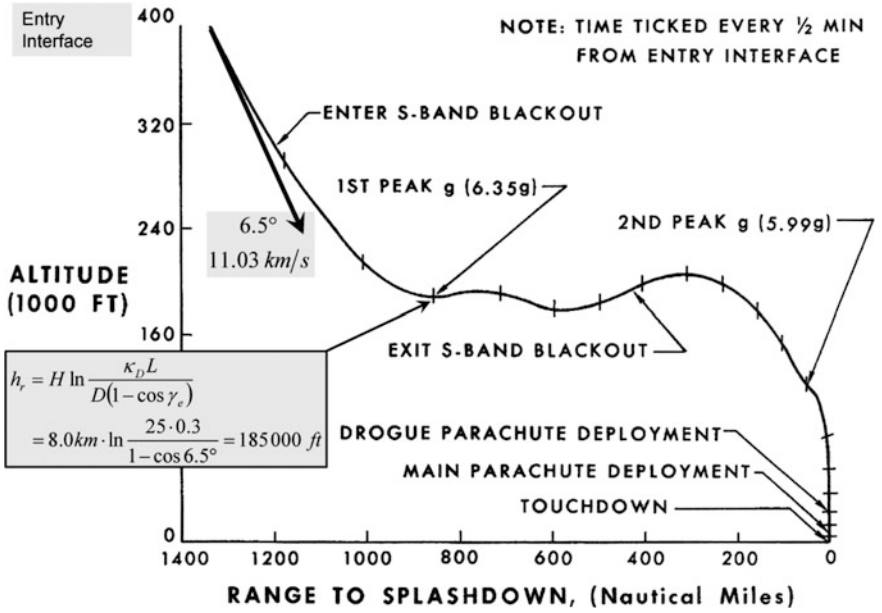

Fig. 10.18 The original reentry trajectory of Apollo 11 with an entry flight inclination angle of 6.5° and reflection at 185,000 ft altitude. *Credit* NASA

10.5.3 Phugoid Mode

It should be obvious now to drive skipping into the extreme and skip not only once but at a very shallow entry angle again and again to slowly but steadily reduce the speed. This indeed would be possible. Any reentry body with $L > 0.5$ at $\varepsilon_e = 1$ and $\gamma_e < 2°$ will experience multiple or continuous skipping. This can be easily verified numerically and is done and displayed in Fig. 10.19 for $L/D = 1.3$ and $\gamma_e = 1.2°$, which were typical entry parameters for the Space Shuttle. The state of such shallow continuous ups and downs is called *hypersonic phugoid mode*. These are oscillatory variations of altitude, where the flight path angle periodically oscillates with decreasing amplitude around zero.

The characteristic feature of a phugoid motion is that the S/C at very high speed and at very flat flight path angle, i.e., $\cos\gamma \approx 1$ and $\sin\gamma \approx \gamma$, oscillates around a mean flight path angle, $\gamma_D = const$, so $\langle\dot{\gamma}\rangle_t \approx 0$. We therefore can approximate the equations for a phugoid motion from the general equations of motion (10.2.1), (10.2.2), and (10.2.3) as

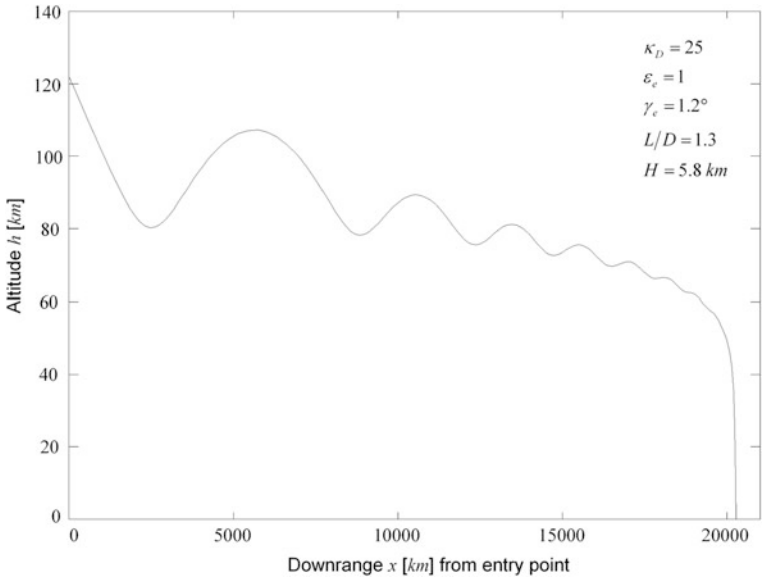

Fig. 10.19 The phugoid oscillation that would result from an uncontrolled lifting reentry of a Space Shuttle ($\gamma_e = 1.2°, L/D = 1.3$). The scale height $H = 5.8$ km is adjusted to the altitude where the phugoid oscillation happens

$$\dot{\gamma} = -\frac{L/v}{m} + \left(\frac{g}{v} - \frac{v}{r}\right)$$
$$\dot{v} = -\frac{D}{m} + g\gamma$$
$$\dot{h} = -v\gamma$$

The oscillations should be noticeable in variations of the flight path angle. In seeking for a differential equation for that we differentiate the above γ equation with respect to time

$$\ddot{\gamma} = -\frac{1}{m}\left(\frac{\partial(L/v)}{\partial h}\dot{h} + \frac{\partial(L/v)}{\partial v}\dot{v}\right) + 0 \cdot \dot{h} - \left(\frac{g}{v^2} + \frac{1}{r}\right)\dot{v}$$

where we have assumed that the oscillations take place at about a constant altitude, $r \approx const$. From Eqs. (10.2.4) to (10.2.5) follows

$$\frac{\partial(L/v)}{\partial h} = -\frac{(L/v)}{H} \quad \text{and} \quad \frac{\partial(L/v)}{\partial v} = \frac{L}{v^2}$$

and therefore

$$\ddot{\gamma} = -\frac{1}{m}\left[\frac{L}{H}\gamma + \frac{L}{v^2}\left(g\gamma - \frac{D}{m}\right)\right] - \left(\frac{g}{v^2} + \frac{1}{r}\right)\left(g\gamma - \frac{D}{m}\right)$$

from which follows

$$\ddot{\gamma} = -\left[\frac{L}{mH} + g\left(\frac{g}{v^2} + \frac{1}{r} + \frac{L}{mv^2}\right)\right]\gamma + \frac{D}{m}\left(\frac{g}{v^2} + \frac{1}{r} + \frac{L}{mv^2}\right)$$

Because it follows from the γ equation with $\langle\dot{\gamma}\rangle_t \approx 0$ and $\cos\gamma \approx 1$ that $v^2 \approx \langle v\rangle_t^2 = r(g - L/m)$, we find

$$\begin{aligned}\frac{g}{v^2} + \frac{1}{r} + \frac{L}{mv^2} &\approx \frac{g}{r(g - L/m)} + \frac{1}{r} + \frac{L}{r(mg - L)} = \frac{1}{r}\frac{mg + mg - L + L}{mg - L} \\ &= \frac{1}{r}\frac{2mg}{mg - L}\end{aligned}$$

Hence

$$\ddot{\gamma} = -\left(\frac{L}{mH} + \frac{2g}{r}\frac{mg}{mg - L}\right)\gamma + \frac{2D}{mr}\frac{mg}{mg - L} \tag{10.5.7}$$

This is the differential equation of a somewhat odd linear oscillator, which we write in the general form

$$\ddot{\gamma} = -\left(\omega_0^2 + \omega_1^2\right)\gamma + c$$

Obviously there are two contributions to the phugoid oscillation with angular frequencies

$$\omega_0 = \sqrt{\frac{L}{mH}} \quad \text{and} \quad \omega_1 = \sqrt{\frac{2g}{r}\frac{mg}{mg - L}} \tag{10.5.8}$$

If we trace back these contributions in the derivation, we see that the oscillation with ω_1 is caused by the causal chain (mode): declining S/C → increasing speed → increasing centrifugal force + increasing lift → decreasing flight path angle → upturn. On the other hand, the ω_0 oscillation stems from the chain: declining S/C → decreasing altitude → exponentially increasing atmospheric pressure → strongly increasing lift → quickly decreasing flight path angle → immediate upturn. We could interpret the latter process also as a bouncing off the atmosphere. These two oscillations happen on quite different time scales. Because

$$\frac{L}{mg} \approx \frac{RL}{mv^2} = \kappa_D \frac{L}{D}\frac{R}{H}e^{-h/H} \approx 0.2$$

it follows

$$\frac{\omega_1^2}{\omega_0^2} \approx \frac{2g}{r} \Big/ \frac{L}{mH} = 2\frac{mg}{L}\frac{H}{r} \approx 2 \cdot 0.2 \cdot 0.001 = 0.0004$$

The short-term ω_0-mode therefore is the more forceful mode by orders of magnitude, which is why we can neglect ω_1. We therefore can simplify Eq. (10.5.7)

$$\ddot{\gamma} = -\omega_0^2\gamma + 2\frac{D}{mr}\frac{mg}{mg - L} = -\omega_0^2(\gamma - \gamma_D)$$

with

$$\gamma_D = 2\frac{D}{L}\frac{H}{r}\frac{mg}{mg - L} \approx 0.1^\circ \tag{10.5.9}$$

To solve the equation we substitute $x := \gamma - \gamma_D$. This implies $\ddot{\gamma} = \ddot{x}$ we therefore get the differential equation $\ddot{x} = -\omega_0^2 x$ with the solution $x = x_0 \cos(\omega_0 t + \varphi)$. By resubstitution and because $\gamma(t = 0) = \gamma_e$ we finally get

$$\gamma = \gamma_D + (\gamma_e - \gamma_D)\cos\omega_0 t \tag{10.5.10}$$

The drag-induced offset $\gamma_D \approx 0.1^\circ$ is the time averaged value of the FPA. It determines the long-term decline of the mean altitude of the vehicle and is easily recognized as such in Fig. 10.19. The period of the phugoid oscillation is determined via Eqs. (10.2.5) and (6.2.17) to be

$$T = \frac{2\pi}{\omega_0} = 2\pi\sqrt{\frac{mH}{L}} = 2\pi\frac{H}{v}e^{\frac{h}{2H}}\sqrt{\frac{D}{\kappa_D L}} \quad \textbf{phugoid period} \tag{10.5.11}$$

So the period decreases exponentially with the altitude at which the phugoid motion takes place. This exponential dependency is nicely depicted in Fig. 10.19. Although the mean flight altitude decreases only slightly with the phugoid motion, the phugoid period (and the mode amplitude) decreases quickly. For a phugoid motion at an altitude of typically $h = 80 - 90$ km ($H \approx 5.8$ km, see Table 6.2) and for $\kappa_L = \kappa_D L/D = 32.5$ the period is $T = 15 - 35$ min.

Because permanent skipping causes a gentle velocity reduction, it may seem ideal, at first glance. However it has a serious drawback: Without any lift control, the downrange distance and with it the landing site can virtually not be determined. Note that in the case of Fig. 10.19 the distance traveled until landing is about

20,000 km, that is half around the globe! This is unacceptable neither for winged bodies and even less for capsules (they have to land on ground or on water with a good accuracy to pick them up), so phugoid modes have to be avoided at any rate. But one can turn the objective upside down. According to an idea of the famous Austrian space engineer Eugen Sänger (1905–1964), it would be possible to design an intercontinental transport high-lift vehicle, the so-called *Antipodal Bomber*, with say, $L/D \approx 2.5$ without any propulsion by accelerating it to LEO speeds and then using wave-like gliding along the surface of the atmosphere to reach a given target point anywhere on the globe with a controllable lift in the late phase. The time required for orbiting the Earth would then be about 1 h 45 min. The critical deceleration at the first reflection would be only 0.1 g, increasing for the following skips until about only 0.4 g in the final phase.

10.6 Lifting Reentry

We have seen that for $\gamma < 2°$ the approximations for a ballistic reentry are no longer valid. For heavy S/Cs, however, reentries at such flat angles are the only way to keep the peak heat load and peak structural load below tolerable values by spreading the deceleration and hence friction over a much longer time period. This can be achieved by an increased L/D of the S/C. This is why all the larger S/Cs are so-called winged bodies, such as the Space Shuttle.

We will now analyze this limiting case of a lifting reentry, where an adjustable lift is utilized to maintain a constant flight path angle, which is typically of the order of 1°. Figure 10.20 shows for instance the target area for the flight path angle at entry interface for a Shuttle reentry. So

$$\dot{\gamma} = 0 \quad \textbf{lifting reentry condition} \tag{10.6.1}$$

Hence $\gamma = \gamma_e \approx 1° = const$. Because of this condition we have: $\sin\gamma = \sin\gamma_e \approx \gamma_e$ and $\cos\gamma \approx 1$. Therefore, the left-hand sides of Eqs. (10.2.2) and (10.2.13b) vanish. In order to have also the right sides zero the following must hold (approximation: $g \approx g_0, r \approx R$)

$$\frac{L}{m} = g - \frac{v^2}{r} \approx g_0\left(1 - \frac{v^2}{v_\triangleright^2}\right) \quad \text{with } v_\triangleright^2 = g_0 R \tag{10.6.2}$$

This equation implies that in course of reentry lift has to be constantly adjusted such that together with the centrifugal force as the other "pulling up" force, they just balance the gravitational force, which "pulls down". This is where the expression *equilibrium glide* (a.k.a. *lifting reentry* or *gliding reentry*) stems from.

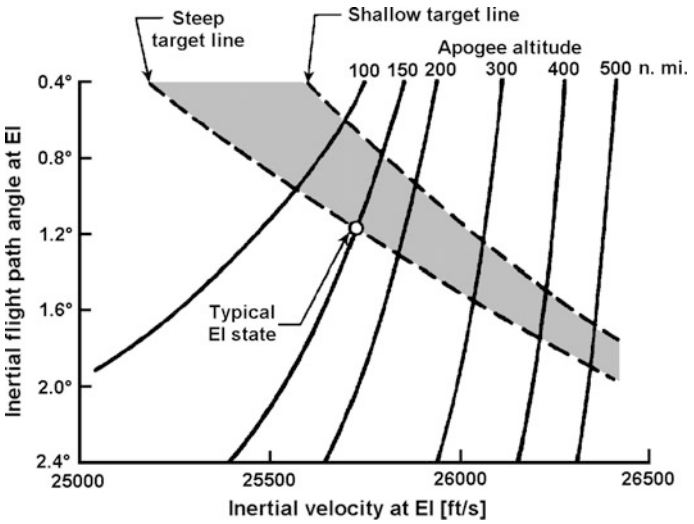

Fig. 10.20 Target area (gray) for the flight path angle at entry interface, EI, for the Space Shuttle. *Credit* N. Chaffee, NASA/JSC

Uncontrolled Lifting Reentry

We already came across lifting reentry when we investigated the phugoid mode. In that case, however, the FPA was not constant at any point in time, but constancy was achieved only on time average:

$$\langle \gamma \rangle_t = \gamma_D = 2\frac{D}{L}\frac{H}{r}\frac{mg}{mg - L} = const$$

Furthermore, the FPA oscillated around this mean value, because we had assumed an unregulated constant L/D ratio.

Controlled Lifting Reentry

The phugoid mode is undesirable for a steady lifting reentry. Therefore a reentry vehicle is required, with $L/D_{\max} \geq 0.7$ and which can adjust lift and drag separately. Lift must be adjustable to such an extent that the phugoid oscillation can be compensated and therefore $\gamma = \gamma_e = const$ can be enforced at any time. This indeed is possible via the so-called *angle of attack* (AOA) α and the so-called *roll angle* (a.k.a. *bank angle*) μ. For the Space Shuttle Fig. 10.23 depicts how drag and lift can be varied jointly by the AOA such that the L/D ratio changes in a way characteristic for the S/C as given in Eq. (10.2.9). Of course for $\alpha = 90°$ $L/D = 0$ always holds, because vertical lift must vanish at that angle. Independent from the AOA a bank angle can be set. The cosine of the bank angle determines the lift component, which points into the z-direction, i.e., upward as shown in Fig. 6.8. It is only this component that balances the gravitational and centrifugal force, and which is

decisive in our equations. If the bank angle is $\mu = 90°$, then the S/C is tilted fully sideways and no upward lift is generated. In summary:

> For a controlled lifting reentry the angle of attack and bank angle of the vehicle are adjusted such that the generated upward lift plus the centrifugal force exactly compensates the gravitational force and hence $\gamma = const$.

10.6.1 Reentry Trajectory

How must L/D be adjusted at a given altitude such that Eq. (10.6.2) is fulfilled? Since we do not know the velocity as a function of altitude for a lifting reentry Eq. (10.6.2) is not a control law for L/D in itself—rather, we have to solve the equation of motion. Applying the condition Eq. (10.6.1) to the basic equations of motion Eq. (10.2.13) we find

$$\begin{aligned} \frac{d(\ln \varepsilon)}{d\lambda} &= -1 + \frac{2H}{\varepsilon \lambda R} \\ \frac{d(\cos \gamma)}{d\lambda} &= \frac{\sin \gamma_e}{2}\frac{L}{D} - \left(\frac{1}{\varepsilon} - 1\right)\frac{H \cos \gamma}{\lambda R} \end{aligned} \qquad \textbf{equations of motion} \qquad (10.6.3)$$

We know already the solution of the γ equation. It is the FPA Eq. (10.4.8). The solution of the decoupled ε equation can be easily derived. We first separate the variables

$$d(\ln \varepsilon) = \left(-1 + \frac{2H}{\varepsilon \lambda R}\right) d\lambda$$

This equation of motion is the same as the one in Sect. 10.4.2 except that here $\gamma = \gamma_e = const \rightarrow c = q = 0$. Therefore, we derive from Eq. (10.4.12) the second-order solutions

$$\begin{aligned} \ln \frac{v}{v_e} &= -\frac{\lambda}{2} + \frac{H}{\varepsilon_e R}\chi(\lambda, 0) \\ \cos \gamma &= \left[1 + \frac{\tan \gamma_e}{2}\frac{L}{D}\lambda - \frac{H}{\varepsilon_e R}\chi(\lambda, \varepsilon_e)\right] \cos \gamma_e \end{aligned} \qquad (10.6.4)$$

The second equation is the FPA Eq. (10.4.8), which also holds for lifting reentry as long as $\tan \gamma_e \cdot \lambda L/(2D) \ll 1$, that is $\exp(h/H) \gg L\kappa_D/D$, i.e., down to about $h = 45$ km. With the FPA equation we have the answer to the question, how to

adjust the lift. Because if for an equilibrium glide $\cos\gamma = \cos\gamma_e = const$ must hold, the last two terms in the square bracket must cancel each other. This condition provides the L/D control law

$$\frac{L}{D} = \frac{2H}{\varepsilon_e R \tan\gamma_e}\frac{\chi(\lambda,\varepsilon_e)}{\lambda} \qquad \textbf{L/D control law} \tag{10.6.5}$$

At very high altitudes, that is for $\lambda_e \ll \lambda < 1$, we can approximate in Eq. (10.6.5) $\chi(\lambda,1) = f^{\lambda} \approx \lambda$ and therefore with $H \approx 7.6$ km and $\varepsilon_e = 1$ we find

$$\frac{L}{D} \approx \frac{2H}{\varepsilon_e R \tan\gamma_e} \approx 0.10 - 0.14$$

This value is much smaller than the typical lift of a winged body, such as the Space Shuttle, which had $L/D \approx 1.0$ at high altitudes, where $\alpha = 40°$ (see Fig. 10.25; Eq. (10.2.10)). Drag has to be as big as possible at very high altitudes, but not to an extent that the flight attitude becomes unstable. Therefore, the AOA is set to the limiting value $\alpha \approx 45°$, while the vertical lift is reduced by a bank angle μ (see Sect. 6.2.5 and note that $L \equiv L_v$ so far, see convention after Eq. (10.2.6)). The bank angle produces horizontal lift, which moves the S/C sideways out of the motion plane, additionally providing cross-range capability (cf. Sect. 10.7.1). To achieve the value $\cos\mu \cdot L/D = 0.10 - 0.14$ we have

$$\mu \approx \arccos(0.12 \mp 0.2) = 83° \pm 1° \tag{10.6.6}$$

Because this is too close to the critical value $\mu = 90°$, where the Space Shuttle would have plunged down, NASA limited the bank angle to $\mu = 80°$ (see Fig. 10.24).

10.6.2 Critical Deceleration

Having found the solutions of the equations of motions it is now straightforward to determine the critical deceleration and those trajectory parameters, namely critical altitude and critical speed, at which it is achieved. Because $\gamma = \gamma_e$, Eq. (10.4.9) is exact and therefore also Eq. (10.4.10). This is true for any entry phases down to the smallest velocities as long as $\gamma = \gamma_e = \gamma_{crit}$. From this we derive the critical altitude

$$\lambda_{crit} = 1 + \frac{2H}{\varepsilon_{crit} R} \quad @ \quad \gamma = \gamma_e = const$$

How big is ε_{crit}? From Eq. (10.6.4) we find that with $H \cdot \chi(\lambda_{crit} \approx 1.0, 0)/R \approx 10^{-3} \ll \lambda_{crit}/2$ follows $\varepsilon_{crit} \approx \varepsilon_e \exp(-\lambda_{crit})$. So for $\lambda_{crit} \approx 1$ we have $\varepsilon_{crit} = \varepsilon_e/e$ and therefore

$$\lambda_{crit} = 1 + \frac{2eH}{\varepsilon_e R} \approx 1 \tag{10.6.7}$$

Thereby we have proven self-consistently that Eq. (10.6.7) is correct. According to Eq. (10.4.15) we find for the critical altitude

$$h_{crit} = H \ln \frac{2\kappa_D}{\sin \gamma_e} \approx 60 \text{ km} \tag{10.6.8}$$

With Eq. (10.6.4) the critical velocity is found to be

$$\ln \frac{v_{crit}}{v_e} = -\frac{1}{2} + \frac{H}{\varepsilon_e R} \chi(1,0)$$

Because

$$\frac{H}{\varepsilon_e R} \chi(\lambda,0) \approx \frac{H}{R} \cdot \frac{h_e - h}{H} = \frac{h_e - h}{R} \approx 0.01$$

we obtain

$$v_{crit} = \frac{v_e}{\sqrt{e}} \left(1 + \frac{H}{\varepsilon_e R} \chi(1,0)\right) \approx \frac{v_e}{\sqrt{e}} = 4.5 \text{ km s}^{-1} \cdot \sqrt{\varepsilon_e} \approx 4.5 \text{ km s}^{-1} \tag{10.6.9}$$

From Eq. (10.4.9) we finally derive the critical deceleration

$$a_{crit} = -\frac{v_\triangleright^2 \sin \gamma_e}{2H} \left[\varepsilon_{crit} \lambda_{crit} - 2\frac{H}{R}\right] \approx -\frac{v_\triangleright^2 \sin \gamma_e}{2H} \varepsilon_{crit} \lambda_{crit} \approx -\frac{v_\triangleright^2 \sin \gamma_e}{2H} \frac{\varepsilon_e}{e}$$

from which follows

$$a_{crit} \approx -\frac{R}{2eH} \sin \gamma_e \cdot g_0 \approx -154 \cdot \sin \gamma_e \cdot g_0 \tag{10.6.10}$$

This equation states that the critical deceleration may take on virtually any value by adjusting the entry angle accordingly. For $\gamma_e = 1.0°$ the deceleration amounts to a modest $a_{crit} = -2.7 \cdot g_0$.

10.6.3 Heat Flux

The structural stress load capacity of the Space Shuttle was about $|a_{crit}| \approx 2.5 \cdot g_0$. Other than this the peak heat load, which via the heat emission corresponds to a peak surface temperature of the heat tiles, is another critical parameter that has to be

taken care of. To determine the peak heat flux we consider Eq. (10.6.2) by applying Eq. (10.2.5)

$$\rho = \rho_0 \frac{H}{\kappa_L R}\left(\frac{v_\triangleright^2}{v^2} - 1\right) = \frac{2}{BR}\frac{D}{L}\left(\frac{v_\triangleright^2}{v^2} - 1\right)$$

where $B = C_D A_\perp / m$ is the ballistic coefficient (see Eq. (6.2.19)). Inserting this into Eq. (10.1.3) we get for the heat flux onto the stagnation point of the vehicle

$$\dot{q}_{S/C} = \frac{St}{2}\sqrt{\rho\rho_q \frac{R_0}{R_n}} \cdot v^3 = \frac{St}{2}\sqrt{\frac{2\rho_q}{BR}\frac{D}{L}\frac{R_0}{R_n}}\sqrt{\frac{v_\triangleright^2}{v^2} - 1} \cdot v^3$$

From the maximum condition

$$\frac{1}{\dot{q}}\frac{d\dot{q}}{dv} = \frac{1}{v\left(v_\triangleright^2/v^2 - 1\right)}\left(2\frac{v_\triangleright^2}{v^2} - 3\right) = 0$$

we finally derive with the critical velocity

$$v_{\max \dot{q}} = v_\triangleright \sqrt{\frac{2}{3}} = 6.1 \text{ km/s} \tag{10.6.11}$$

Remark *If we would have assumed the Detra and Hidalgo heat flux model with* $\dot{q}_{S/C} \propto \sqrt{\rho}\, v^{3.15}$ *we would have derived for the critical velocity* $v_{\max \dot{q}} = v_\triangleright \sqrt{2.15/3.15}$*, which deviates by only 1% from the above result.*

To find the altitude at which the peak heat load is achieved we consider Eq. (10.6.4). Since $v_{\max \dot{q}}$ is about the same as for the ballistic reentry we expect the peak heat load at about 50 km altitude at which λ is of order unity. Because from the above the term $H\chi(\lambda, 0)/(\varepsilon_e R)$ is negligible, $v = v_e e^{-\lambda/2}$ holds at these altitudes. We therefore get for a lifting reentry from LEO, $v_e \approx v_\triangleright$, $\lambda_{\max \dot{q}} = -\ln(2/3)$ and because of Eq. (10.2.12)

$$h_{\max \dot{q}} = H \ln \frac{4.933 \cdot \kappa_D}{\sin \gamma_e} = h_{crit} + 0.90H \quad @ \quad v_e \approx v_0 \tag{10.6.12}$$

For a typical $\gamma_e = 1^\circ$ and $\kappa_D = 25$ we find $h_{\max \dot{q}} \approx 68$ km $\approx h_{crit} + 6.9$ km (cf. Eq. (10.3.15) and Fig. 10.10 for a ballistic reentry).

For the wanted peak heat flux to the S/C we find

$$\dot{q}_{S/C,\max} = \frac{St}{2}\sqrt{\frac{2\rho_q}{BR}\frac{D}{L}\frac{R_0}{R_n}}\frac{2}{3\sqrt{3}}v_\triangleright^3 = \dot{q}_e\frac{2}{3}\sqrt{\frac{2}{3\rho_e BR}\frac{D}{L}\frac{R_0}{R_n}} \tag{10.6.13}$$

with $\dot{q}_e = \frac{St}{2}\sqrt{\rho_q\rho_e}v_\triangleright^3 = 1.15$ W cm^{-2} the standard heat flux at entry interface where $St = 0.001, v_\triangleright = 7.905$ km s^{-1}, $R_0 = 1$ m, $\rho_q = 0.121$ kg m^{-3}, and $\rho_e = 1.80 \times 10^{-8}$ kg m^{-3} the mean atmospheric density at entry interface according to MSIS-E-90. Observe that the heat flux at the stagnation point is reduced by a larger radius of curvature, R_n. However, contrary to the ballistic case (see Sect. 10.3.3) the heat flux no longer depends on the drag coefficient, but on the lift coefficient because the ballistic coefficient $B \propto C_D \propto D$ (see Eqs. (6.2.19) and (10.2.4)). Note that the expression $\rho_e BR$ and hence the entire square root is dimensionless. Note also that $\rho_e BR$ relates to the Bstar B^* of NORAD's TLE (see Remark in Sect. 12.7.3) as

$$\rho_e BR = 2B^*\frac{\rho_e}{\rho_{120}} = 1.46B^*$$

where the latter holds only if the actual atmospheric density at entry interface is the standard value $\rho_{120} \equiv \rho_0 = 2.461 \times 10^{-8}$ kg m^{-3} as assumed in the Simplified General Perturbation Model SGP of NORAD.

With this and with Eq. (10.1.1) the peak temperature load at the stagnation point of the S/C can be determined to be

$$\boxed{T_{\max}^4 = \frac{T_e^4}{\varepsilon}\cdot\frac{2}{3}\sqrt{\frac{2}{3\rho_e BR}\frac{D}{L}\frac{R_0}{R_n}}} \tag{10.6.14}$$

with

$$T_e = \left(\frac{\dot{q}_e}{\sigma}\right)^{1/4} = 671 \text{ K}$$

the standard stagnation point temperature at entry interface and $\varepsilon \approx 0.85$ the approximate emissivity of the heat shield. With Eq. (10.6.13) we can rewrite Eq. (10.1.3) as a normalized equation for the heat flux onto the stagnation point of the S/C as

$$\frac{\dot{q}_{S/C}}{\dot{q}_{S/C\,\max}} = \frac{3\sqrt{3}}{2}\sqrt{(e^\lambda - 1)e^{-3\lambda}} \tag{10.6.15}$$

This function is plotted in Fig. 10.21 for various entry angles.

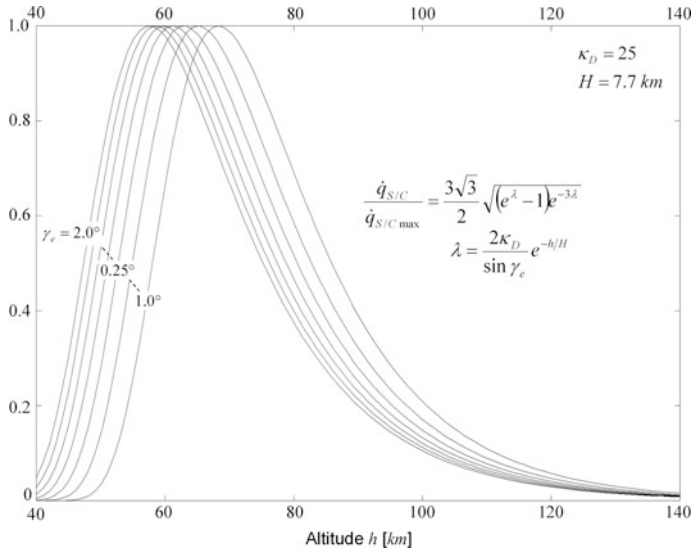

Fig. 10.21 Normalized heat flux at the stagnation point of a spacecraft with lifting reentry as a function of altitude h and entry angle γ_e in steps of 0.25°

10.7 Space Shuttle Reentry

Having investigated so far the challenges of a reentry, we now want to exemplify the practical solution in a case study, namely the Space Shuttle reentry. The detailed figures of the reentry profile described hereafter are taken from the reentry of my Shuttle mission STS-55 on May 6, 1993. However, the reentry profile applies quantitatively to all Shuttle reentries and qualitatively to any winged body's reentry.

The preferred diagram to represent reentry constraint boundaries and hence to formulate guidance control would be the dynamic pressure state versus velocity state space. However, this would require deriving the dynamic pressure from vehicle acceleration and altitudes and to have lift and drag coefficient models for all angles of attack and Mach numbers. Because such relationships would include considerable uncertainties, the constrained boundaries are usually reformulated into a drag acceleration state versus Earth relative velocity state space diagram (see Fig. 10.22). This formulation requires only an estimate of L/D as a function of AOA, which is well known (see Eq. (10.2.9)), and drag acceleration, which is easily measured as an acceleration force normal to the trajectory.

Note that here, in the following, and quite generally in NASA terminology "drag acceleration" means "vehicle deceleration due to drag", i.e. $-\dot{v}_D$, which according to Eq. (10.2.1) is $-\dot{v}_D = D/m$, i.e. mass-specific drag itself.

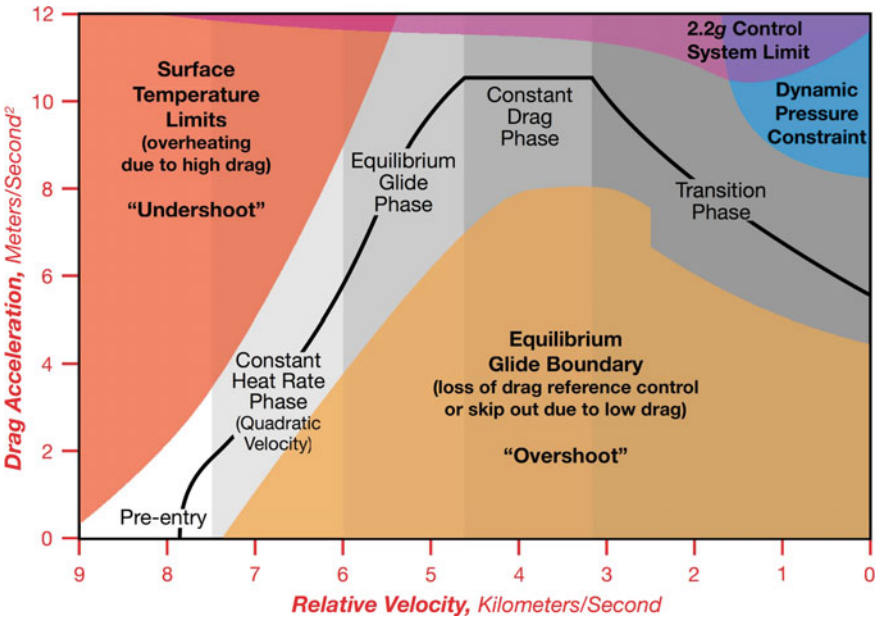

Fig. 10.22 The Shuttle reentry profile in the drag acceleration/Earth relative velocity state space (cf. Fig. 10.1). The Shuttle entered the diagram at high velocity and crossed it on the bold line from left to right within the so-called "flight corridor" (gray area). *Credit* M. Tigges, R. Rohan/NASA

Starting from the deorbit burn, the Shuttle traversed seven different reentry phases: the deorbit phase; the five aerodynamic phases as depictured in Fig. 10.22: pre-entry phase, constant heat phase, equilibrium phase, constant drag phase, and transition phase; and finally the Terminal Area Energy Management (TAEM) phase. We will walk through all these phases in the following sub-sections. The reentry profile described hereafter is taken from the reentry of my mission STS-55 on May 6, 1993, but is typical for the lifting reentry of any kind of winged body.

Deorbit Phase

Typically, a Shuttle resides in an circular LEO orbit at altitude $h_i = 300$ km. Sixty minutes and forty seconds before touchdown, and with it 170° west of the touchdown point, it executes a deorbit burn of 176 s duration to reduce the orbital velocity of 7.73 km s^{-1} by just 0.0885 km s^{-1} (i.e., by only 1.1%!—see Shuttle reentry example in Sect. 10.1.3). This brings the Shuttle on an entry ellipse, on which it descends. After 28 min it crosses the entry interface at an altitude of 122 km with $\gamma_e = 1.2°$ and $v_e = 7.86$ km s^{-1} (generally 1.0°–1.5° and 7.82 − 7.89 km s^{-1}).

10.7.1 Reentry Flight Design and Pre-entry Phase

Beyond the entry point down to Mach 14, the primary goal is to avoid unacceptable aerothermodynamic heating, especially on the upper surface and wing leading edge. To accomplish this, the Shuttle is placed at an AOA (angle of attack) of about $\alpha = 40°$ (see Fig. 10.23). The air molecules, which can be considered ballistic at these altitudes, collide with the large bottom side of the Shuttle thus transferring more momentum and hence causing also more desired drag.

But at the same time and according to Eq. (6.2.27) they cause increased lift. This is undesirable as in this phase of almost free fall gravitational force and centrifugal force balance each other. So, an upward lift would bring about skipping. To avoid this, the S/C is tilted sideways (see Sect. 6.2.5) with a bank angle of $\mu \leq 80°$ (see Fig. 10.24) at an unaltered AOA, so that the Shuttle is in a sloping lateral attitude with very low vertical lift. This is in line with our *L/D* control law from Eq. (10.6.5). NASA limits the bank angle to 80°, because any uncontrollable slight increase beyond 80° would lead to the Space Shuttle plunging straight down. The technical term of this roll maneuver is "roll reversals" or "bank reversals" because they are carried out alternately to the left and right side.

During a bank reversal, which can last up to 1 min, the lift may become very large, in particular at the moment when the bank angle is about zero. This would immediately induce a skipping action. To avoid this, the AOA is simultaneously increased during the bank reversal so that lift increases not too much (cf. Fig. 10.25). Thereby the drag increases insignificantly.

An additional benefit of roll reversals is that they allow lateral steering of the Space Shuttle, which at this very early reentry phase increases the cross-range capability to about 2000 km. This is highly desirable to ensure that the Shuttle reaches the landing site (see Fig. 10.26) and still has sufficient range capability to properly align with the runway heading (see TAEM phase Sect. 10.7.6). Roll maneuvers are continually carried out during reentry right down to Mach 2.5.

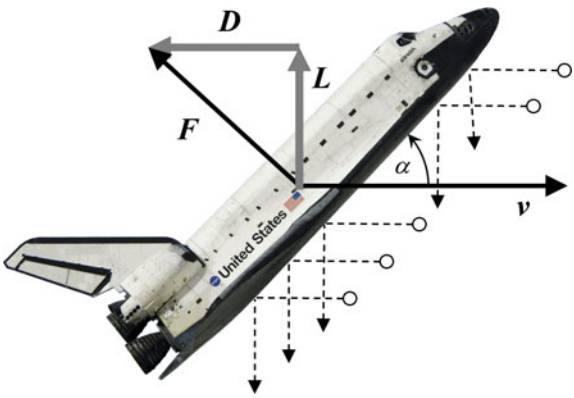

Fig. 10.23 Drag and lift of a Space Shuttle at a typical $AOA = \alpha = 40°$ in the early reentry phases

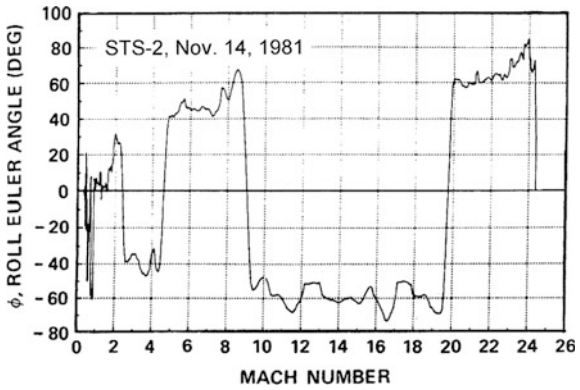

Fig. 10.24 Bank angle as a function of entry velocity. *Credit* P. Romere, C. Young (1983), NASA/AIAA

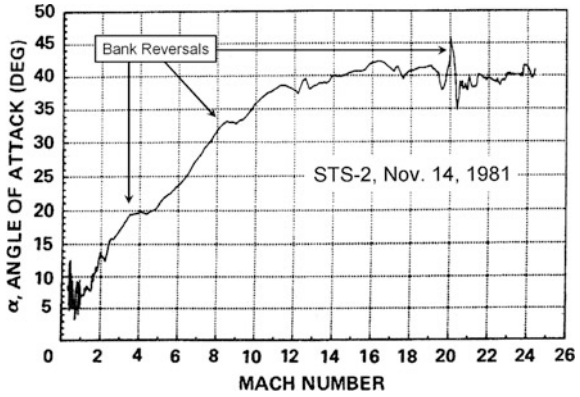

Fig. 10.25 AOA profile as a function of entry velocity. *Credit* P. Romere, C. Young (1983), NASA/AIAA

The guidance control algorithm has two objectives: To guide the Shuttle through the flight corridor (see Fig. 10.22) and at any given moment to compute how far the vehicle could fly. i.e. whether it could reach the runway. Any difference between the analytically computed range and the required range would trigger an adjustment in the drag-velocity references to remove that range error. Thus it made use of the tolerances of the flight corridor to remove range errors.

Pre-entry Phase

In this sloping lateral attitude the Shuttle flies at a roughly constant velocity of $v = 7.9$ km s^{-1} (cf. Fig. 10.7) down to an altitude of about 80 km. So, drag merely reduces its potential energy. In this phase the two primary parameters to control the vehicle's attitude and thus lift and drag and also the desired range and cross-range during reentry are AOA (set by the body flap) and bank angle (set by the ailerons and aft yaw Reaction Control System jets).

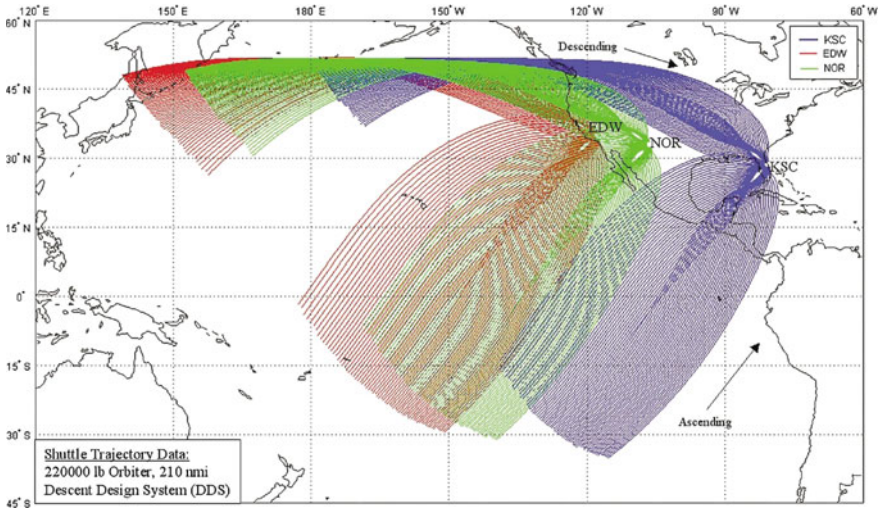

Fig. 10.26 Possible reentry ground tracks from 51.6° orbit inclination (ISS). Blue lines are landing at Kennedy Space Center (KSC), green at White Sands Space Harbor, Northrup Strip (NOR), and red at Edwards Air Force Base (EDW). *Credit* NASA

10.7.2 Constant Heat Rate Phase (Thermal Control Phase)

At about 80 km altitude the heat flux is 70% of its maximum value (see Fig. 10.21), so that from now on the heat rate needs to be controlled by vehicle guidance. This is the constant heat rate phase of the reentry profile, which extends from altitudes 80–50 km and in which the Shuttle retains its *AOA* of about 40°. At these altitudes the thermal shield of the Shuttle heats up so much that the impacting air around the Shuttle ionizes forming a plasma, which is impermeable for electromagnetic waves. For about 15 min there is no radio communication with Mission Control. That is why this phase is called the "blackout phase". The drag is now so strong that velocity is fiercely reduced.

A constant heat rate was achieved by assuming two consecutive segments with a heuristic quadratic velocity profile for drag acceleration (= drag)

$$D = c_1 + c_2 v + c_3 v^2$$

with constants c_1, c_2, c_3 that empirically determine the bold line in the flight corridor of Fig. 10.22. Deviations from this reference drag profile are counteracted by modulations of the *AOA* of around 40°. This heat control procedure limits the heat flux such that it does not peak as depicted in Fig. 10.21 for an equilibrium glide, but plateaus the heat flux and hence also the maximum temperature at the stagnation point. This effect can be seen from the temperature profile of the nose cap of the Shuttle in Fig. 10.27.

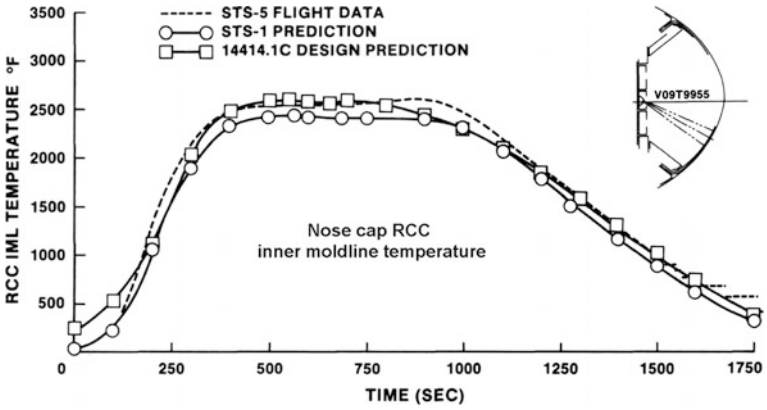

Fig. 10.27 Nose cap RCC inner moldline temperature as a function of time after entry interface. *Credit* NASA

10.7.3 Equilibrium Glide Phase

As the Shuttle speed drops below 6.2 km/s, the constant heat rate phase ends and the equilibrium glide phase begins. This should be considered as an intermediate phase between heating and rapidly increasing deceleration forces as the vehicles penetrated deeper into the atmosphere. It is an uncritical phase because according to Fig. 10.22 the flight corridor widens. Nevertheless, the glide slope guidance is designed to reserve range capability.

Apart from the altitude-dependent flight profile, which we had discussed in Sect. 10.4.2, it is possible to provide for this flight phase a time-dependent expression for the key trajectory parameters. To do so we consider the equations of motion in the time-dependent form as given by Eq. (10.2.1) with $\cos\gamma \approx 1, \sin\gamma \approx 0$ and Eq. (10.6.2)

$$\dot{v} = -\frac{D}{m} \tag{10.7.1}$$

$$\frac{L}{m} = g_0\left(1 - \frac{v^2}{v_\triangleright^2}\right), v_\triangleright = 7.905 \text{ km s}^{-1}$$

and therefore the drag-velocity profile for guidance and control

$$D = \frac{mg_0}{L/D}\left(1 - \frac{v^2}{v_\triangleright^2}\right)$$

We eliminate m from both equations, and get

$$\dot{v} = a = -g_0 \frac{D}{L}\left(1 - \frac{v^2}{v_\triangleright^2}\right) \tag{10.7.2}$$

Note that $v < v_\triangleright$ is mandatory, as for $v > v_\triangleright$ we would get $\dot{v} > 0$, i.e., the Shuttle would accelerate rather than decelerate. Separating the variables in Eq. (10.7.2) results in

$$\int_{v_e/v_0}^{v/v_0} \frac{dx}{1-x^2} = \operatorname{arctan\,h}\frac{v}{v_\triangleright} - \operatorname{arctan\,h}\frac{v_e}{v_\triangleright} = -\frac{g_0}{v_\triangleright}\int_0^t \frac{D}{L}dt = -\frac{Dg_0}{Lv_\triangleright}t$$

Because of the constant AOA, $D/L = const$ is valid during that flight phase, and we can extract this term from the integral. After some modifications, we get

$$v = v_e \frac{1 - \frac{v_\triangleright}{v_e}\tanh\left(\frac{\alpha t}{v_\triangleright}\right)}{1 - \frac{v_e}{v_\triangleright}\tanh\left(\frac{\alpha t}{v_\triangleright}\right)} \quad \text{with } \alpha := g_0\frac{D}{L} \tag{10.7.3}$$

To see that v indeed decreases, we expand this equation into a power series of $\alpha t \ll v_\triangleright$ for small time periods (exercise, Problem 10.7) and for $v_e < v_\triangleright$

$$v = v_e - \alpha t\left(1 - \frac{v_e^2}{v_\triangleright^2}\right)\left[1 + \frac{v_e}{v_\triangleright^2}\alpha t - \frac{\alpha^2 t^2}{v_\triangleright^2}\left(\frac{1}{3} - \frac{v_e^2}{v_\triangleright^2}\right) + \cdots\right] \tag{10.7.4}$$

We recognize that velocity decreases at an increasing rate. The corresponding deceleration is found by differentiating Eq. (10.7.4)

$$a = -\alpha\left(1 - \frac{v_e^2}{v_\triangleright^2}\right)\left[1 + \frac{2v_e}{v_\triangleright^2}\alpha t - \frac{1}{v_\triangleright^2}\alpha^2 t^2\left(1 - 3\frac{v_e^2}{v_\triangleright^2}\right) + \cdots\right] \tag{10.7.5}$$

The acceleration increases monotonously over time. For a winged body with $L/D = 1.3$, such as the Shuttle, Eqs. (10.7.4) and (10.7.5) have an inaccuracy of about 10% after 15 min, so they are sufficiently accurate over the entire blackout phase.

10.7.4 Constant-Drag Phase

The equilibrium phase passes into the constant drag phase when the maximum drag acceleration of 10 m/s^2 occurs, or if a velocity of 4.6 km/s is achieved, which typically happens at an altitude of about 50 km. Because of the further increasing atmospheric density, the Space Shuttle comes now into a fully aerodynamic state. With a still decreasing velocity the absolute value of the deceleration increases to $1.5\,g_0$ according to Eq. (10.7.2). In order to limit the stress load to the Shuttle and the crew, the drag deceleration now is curbed to $D/m = -a = 1.5\,g_0$ This is achieved at steadily decreasing velocities, according to Eq. (10.2.9) and Eq. (10.7.2), by increasing L/D and hence decreasing AOA = α according to

$$\frac{\sin\alpha\sin 2\alpha}{2\sin^3\alpha + 0.045} = \frac{L}{D} = \frac{1}{1.5}\left(1 - \frac{v^2}{v_\triangleright^2}\right) \quad @ \quad D/m = -\dot{v} = 1.5\, g_0 \qquad (10.7.6)$$

Thus the AOA is constantly reduced from 40° down to about 33° at Mach 9. It is during this phase that the velocity falls below Mach 11 where the Shuttle leaves the blackout phase.

10.7.5 Transition Phase

Owing to the strongly increasing atmospheric density the dynamic pressure and hence the load factor on the Shuttle increases so that starting at a speed of 3.2 km/s the drag deceleration has to be reduced. This is achieved by further reducing the AOA to 8° at Mach 1 (see Fig. 10.25). According to Eq. (10.2.9) a decreasing AOA increases L/D. Due to a much reduced velocity, the flight-path angle becomes significantly steeper and the flight strongly aerodynamic. This influences the formulation of the Shuttle AOA guidance from a drag-velocity to a drag-energy profile of the form

$$D = D_F + c_5(E - E_F)$$

where $E = \frac{1}{2}mv^2 + mgh$ is the total vehicle energy, c_5 is an empirical parameter derived from range requirements, and index F indicates final values at the transition to the TAEM phase, namely an altitude of about 25 km at Mach 2.5. This delivers the spacecraft to the desired energy state at TAEM interface. Up to this point the Shuttle has covered a distance of 8000 km in 54 min.

10.7.6 TAEM Phase

The Shuttle enters the final phase, the so-called Terminal Area Energy Management (TAEM) phase (see Fig. 10.28), with Mach 2.5 at 25 km altitude and a distance of about 90 km from the runway. During the remaining 6 min the Shuttle undergoes flight maneuvers with changing $AOA = 4° - 10°$ to align velocity and heading to the approach cone of the landing strip. At Mach 1, about 4 min prior to touch down, the commander takes manual control of the spacecraft's approach. The glide path angle ($\gamma = 17° - 19°$) in the landing phase is six times bigger than that of a commercial aircraft, and the touch down velocity $v = 335$ km h^{-1} is about twice as high.

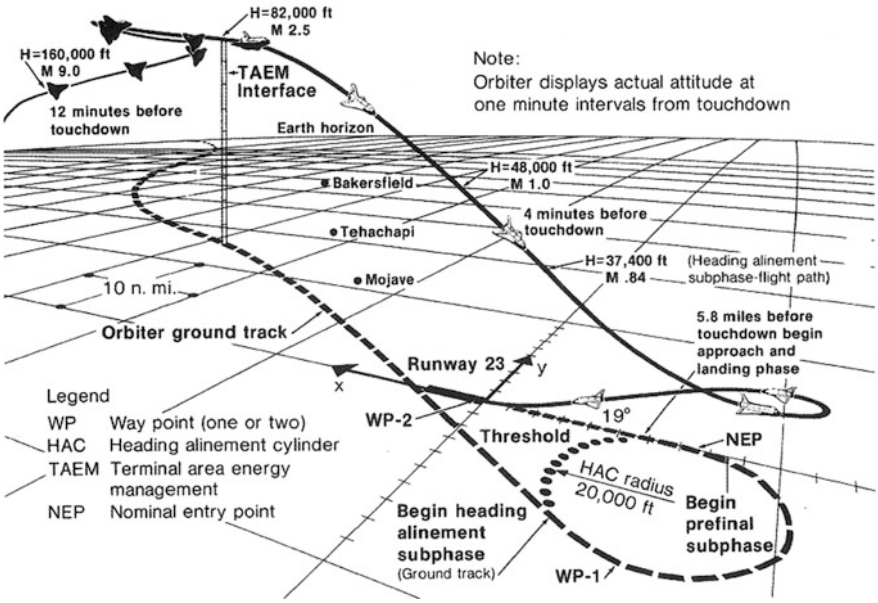

Fig. 10.28 STS-3 TAEM entry profile to Edwards Airforce Base. *Credit* NASA

10.8 Problems

Problem 10.1 *LEO Deorbit*
Prove Eq. (10.1.11).

Problem 10.2 *Normalized Equations of Motion*
From the equations of motions (10.2.1), (10.2.2), and (10.2.3) derive the normalized equations of motion (10.2.7).

Problem 10.3 *Reduced Equations of Motion*
From the equations of motions (10.2.1), (10.2.2), and (10.2.3) derive the reduced equations of motions (10.2.13) through the variable substitution $dt \rightarrow d\lambda$.

Problem 10.4 *Low-Lift Reentry Trajectory*
Prove the low-lift reentry trajectory, Eq. (10.4.13).

Hint: Derive the first-order differential equation of the trajectory equation from $\dot{h} = -v\sin\gamma$ and $\dot{x} = v\cos\gamma$.

Problem 10.5 *Subsonic Gliding Angle*
Show from the equations of motion that for reentry vehicles with a substantial lift the glide path angle in the terminal subsonic gliding phase where $\dot{v} \ll g\sin\gamma$ becomes

$$\tan\gamma = \frac{D}{L}$$

Problem 10.6 *High-Lift Reentry*
We assume a high-lift reentry.

(a) Show that for the reflection phase where gravitation is negligible and hence $H/R \to 0$ the exact solutions to the equations of motion

$$\frac{d\varepsilon}{d\lambda} = -\frac{\sin\gamma_e}{\sin\gamma}\varepsilon$$
$$\frac{d(\cos\gamma)}{d\lambda} = \frac{\sin\gamma_e}{2}\frac{L}{D}$$

read

$$\cos\gamma = \cos\gamma_e\left[1 + \frac{\tan\gamma_e}{2}\frac{L}{D}(\lambda - \lambda_e)\right]$$

and

$$\ln\frac{\varepsilon}{\varepsilon_e} = -2\frac{D}{L}\left[\arcsin\left(\cos\gamma_e + \frac{\sin\gamma_e}{2}\frac{L}{D}(\lambda - \lambda_e)\right) - \arcsin(\cos\gamma_e)\right]$$

(b) Using the functional approximation

$$\arcsin(\cos\alpha + x\sin\alpha) - \arcsin(\cos\alpha) = x + \frac{1}{2}\cot\alpha \cdot x^2$$
$$+ \frac{1}{2}\left(\frac{1}{3} + \cot^2\alpha\right)x^3 + \cdots$$

for $x \to 0$ prove that the latter solution passes over into

$$\ln\frac{\varepsilon}{\varepsilon_e} = -(\lambda - \lambda_e) - \frac{1}{4}\frac{L}{D}\cot\gamma_e(\lambda - \lambda_e)^2$$

and hence is in accordance with Eq. (10.4.4) for $c \to 0$ and Eq. (10.4.12).

Problem 10.7 *Deceleration in Blackout Phase*
Prove Eq. (10.7.4) from Eq. (10.7.3) for $\alpha t \ll v_\triangleright$.